Detailed structure of ^{131}Sn populated in the β decay of isomerically purified ^{131}In states

J. Benito[1,*] L. M. Fraile,[1,†] A. Korgul,[2] M. Piersa-Siłkowska,[2,3] A. Jaries,[4] A. Stryjczyk,[2,5,4] E. Adamska,[2]
R. Álvarez-Rodríguez,[6] A. N. Andreyev,[7,8] A. E. Barzakh,[9] G. Benzoni,[10] T. Berry,[11] M. J. G. Borge,[3,12] M. Carmona,[1]
K. Chrysalidis,[3] C. Costache,[13] J. G. Cubiss,[3,7] T. Day Goodacre,[3,14] H. De Witte,[5,3] T. Eronen,[4] D. V. Fedorov,[9]
V. N. Fedosseev,[3] G. Fernández-Martínez,[15] A. Fijałkowska,[2] M. Fila,[2] H. Fynbo,[16] D. Galaviz,[17] P. Galve,[1] M. García-Díez,[1]
Z. Ge,[4] P. T. Greenlees,[4,18] R. Grzywacz,[19,20] C. Henrich,[15] M. Huyse,[5] P. Ibáñez,[1] A. Illana,[5,21,‡] Z. Janas,[2] J. Jolie,[22]
D. S. Judson,[23] A. Kankainen,[4] V. Karayonchev,[22] M. Kicińska-Habior,[2] J. Konki,[4,18] J. Kurcewicz,[3] I. Lazarus,[24] R. Lică,[3,13]
A. López-Montes,[1] M. Lund,[16] H. Mach,[25,§] M. Madurga,[3,19] N. Mărginean,[13] R. Mărginean,[13] I. Marroquín,[12] B. A. Marsh,[3,§]
M. C. Martínez,[1] C. Mazzocchi,[2] K. Miernik,[2] C. Mihai,[13] R. E. Mihai,[13] M. Mougeot,[4] J. R. Murias,[1] E. Nácher,[26]
A. Negret,[13] B. Olaizola,[27,12] R. D. Page,[23] S. V. Paulauskas,[19] S. Pascu,[13] A. Perea,[12] V. Pucknell,[24] A. Raggio,[4] P. Rahkila,[4,18]
C. Raison,[7] E. Rapisarda,[3] J.-M. Régis,[22] K. Rezynkina,[5,28] F. Rotaru,[13] S. Rothe,[3] J. Ruotsalainen,[4] D. Sánchez-Parcerisa,[1]
V. Sánchez-Tembleque,[1] K. Schomacker,[22] G. S. Simpson,[29] Ch. Sotty,[13,5] L. Stan,[13] M. Stănoiu,[13] O. Tengblad,[12]
A. Turturica,[13] J. M. Udías,[1] P. Van Duppen,[5] V. Vedia,[1] A. Villa-Abaunza,[1] S. Viñals,[12] R. Wadsworth,[7]
W. B. Walters,[30] and N. Warr[22]

(IDS and IGISOL Collaboration)

[1]*Grupo de Física Nuclear & IPARCOS, Universidad Complutense de Madrid, CEI Moncloa, E-28040 Madrid, Spain*
[2]*Faculty of Physics, University of Warsaw, PL 02-093 Warsaw, Poland*
[3]*CERN, CH-1211 Geneva 23, Switzerland*
[4]*University of Jyvaskyla, Department of Physics, Accelerator Laboratory, P. O. Box 35(YFL) FI-40014 University of Jyvaskyla, Finland*
[5]*Instituut voor Kern- en Stralingsfysica, KU Leuven, B-3001 Leuven, Belgium*
[6]*Escuela Técnica Superior de Arquitectura, Universidad Politécnica de Madrid, E-28040 Madrid, Spain*
[7]*School of Physics, Engineering and Technology, University of York, YO10 5DD York, United Kingdom*
[8]*Advanced Science Research Center (ASRC), Japan Atomic Energy Agency, Tokai-mura, Naka-gun, Ibaraki 319-1195, Japan*
[9]*Affiliated with an institute covered by a cooperation agreement with CERN*
[10]*Istituto Nazionale di Fisica Nucleare, Sezione di Milano, I-20133 Milano, Italy*
[11]*Department of Physics, University of Surrey, Guildford GU2 7XH, United Kingdom*
[12]*Instituto de Estructura de la Materia, CSIC, E-28040 Madrid, Spain*
[13]*"Horia Hulubei" National Institute of Physics and Nuclear Engineering, RO-077125 Bucharest, Romania*
[14]*School of Physics and Astronomy, The University of Manchester, M13 9PL Manchester, United Kingdom*
[15]*Institut für Kernphysik, Technische Universität Darmstadt, D-64289 Darmstadt, Germany*
[16]*Department of Physics and Astronomy, Aarhus University, DK-8000 Aarhus C, Denmark*
[17]*LIP, and Faculty of Sciences, University of Lisbon, 1000-149 Lisbon, Portugal*
[18]*Helsinki Institute of Physics, University of Helsinki, FIN-00014 Helsinki, Finland*
[19]*Department of Physics and Astronomy, University of Tennessee, Knoxville, Tennessee 37996, USA*
[20]*Physics Division, Oak Ridge National Laboratory, Oak Ridge, Tennessee 37831, USA*
[21]*Instituto Nazionale di Fisica Nucleare, Laboratori Nazionali di Legnaro, I-35020 Legnaro, Italy*
[22]*Institut für Kernphysik, Universität zu Köln, D-50937 Köln, Germany*
[23]*Department of Physics, Oliver Lodge Laboratory, University of Liverpool, Liverpool L69 7ZE, United Kingdom*
[24]*STFC Daresbury, Daresbury, Warrington WA4 4AD, United Kingdom*
[25]*National Centre for Nuclear Research, PL 02-093 Warsaw, Poland*
[26]*Instituto de Física Corpuscular, CSIC - Universidad de Valencia, E-46071 Valencia, Spain*
[27]*TRIUMF, Vancouver, British Columbia, V6T 2A3 Canada*
[28]*Istituto Nazionale di Fisica Nucleare, Sezione di Padova, I-35131 Padova, Italy*
[29]*LPSC, IN2P3-CNRS/Université Grenoble Alpes, Grenoble Cedex F-38026, France*
[30]*Department of Chemistry, University of Maryland, Maryland 20742, USA*

---

*Contact author: jabenito@ucm.es

†Contact author: lmfraile@ucm.es

‡Present address: Grupo de Física Nuclear & IPARCOS, Universidad Complutense de Madrid, CEI Moncloa, E-28040 Madrid, Spain.

§Deceased.

The excited structure of the single-hole nucleus ^{131}Sn populated by the β^- decay of ^{131}In was investigated in detail at the ISOLDE facility at CERN. This new experiment took advantage of isomeric purification capabilities provided by resonant ionization, making it possible to independently study the decay of each isomer for the first time. The position of the first-excited $\nu h_{11/2}$ neutron-hole state was confirmed via an independent mass spectroscopy experiment performed at the Ion Guide Isotope Separator On-Line facility at the University of Jyväskylä. The level scheme of ^{131}Sn was notably expanded with the addition of 31 new γ-ray transitions and 22 new excited levels. The γ-emitting excited levels above the neutron separation energy in ^{131}Sn were investigated, revealing a large number of states, which in some cases decay by transitions to other neutron-unbound states. Our analysis showed the dependence between the population of these states in ^{131}Sn and the β-decaying ^{131}In state feeding them. Profiting from the isomer selectivity, it was possible to estimate the direct β feeding to the $3/2^+$ ground and $11/2^-$ isomeric states, disentangling the contributions from the three indium parent states. This made possible to resolve the discrepancies in $\log ft$ for first-forbidden transitions observed in previous studies, and to determine the β-delayed neutron decay probability (P_n) values of each indium isomers independently. The first measurement of subnanosecond lifetimes in ^{131}Sn was performed in this work. A short $T_{1/2} = 18(4)$-ps value was measured for the $1/2^+$ neutron single-hole 332-keV state, which indicates an enhanced l-forbidden $M1$ behavior for the $\nu 3s_{1/2}^{-1} \rightarrow \nu 3d_{3/2}^{-1}$ transition. The measured half-lives of high-energy states populated in the β decay of the $(21/2^+)$ second isomeric state (^{131m2}In) provided valuable information on transition rates, supporting the interpretation of these levels as core-excited states analogous to those observed in the doubly-magic ^{132}Sn.

I. INTRODUCTION

The investigation of nuclear structure around ^{132}Sn is crucial for the understanding of the evolution of single-particle states in neutron-rich nuclei in the vicinity of nuclear shell closures. The isotope ^{132}Sn with $Z = 50$ and $N = 82$ is one of the best examples of a doubly-magic nucleus [1–4] and is the heaviest radioactive doubly-magic nucleus for which spectroscopic information is available not only for ^{132}Sn but also for its one-particle and one-hole neighbors. This is of importance since it makes it possible to experimentally access single-particle states around the $Z = 50$ and $N = 82$ shell closures [5–8]. Particle-hole excitations also play an important role in ^{132}Sn and neighboring nuclei, since they provide insight into the subtle interplay between single-particle degrees of freedom and collective behavior [9–11] and may provide indications on the robustness of the underlying shell closures.

Exotic nuclei in the ^{132}Sn region also have an impact on the r-process nucleosynthesis path, since the crossing of the $N = 82$ shell closure defines the neutron capture waiting points and shapes the second peak in the chart of natural abundances of chemical elements [12–15]. Nuclear masses, neutron separation energies, β-delayed neutron emission, and neutron capture rates are not only important for the competition of neutron captures and β decays [16] but also to predict nuclear properties far from stability, which are then employed in r-process calculations spanning regions that are experimentally out of reach. In addition to the decay rates and reaction properties, the level structures of nuclei in the region play a role on the predicted neutron-capture cross sections [17].

The nucleus ^{131}Sn, with $Z = 50$ and $N = 81$, one neutron fewer than the doubly-magic ^{132}Sn, is the subject of this work. It is especially relevant to identify the single-neutron hole states in ^{132}Sn, which are basic empirical ingredients for the nuclear shell model [18,19]. While most single-particle and single-hole states for both protons and neutrons have been gradually found in experiment [2,5–8,20–23], the precise position of the single-hole $\nu h_{11/2}^{-1}$ state remains to be firmly established. The low energy of this state with respect to the $\nu d_{3/2}^{-1}$ ground state (g.s.) is the main cause of the existence of β-decaying isomers in the $N = 81$ isotones. Both low-lying $d_{3/2}^{-1}$ and $h_{11/2}^{-1}$ neutron states have been experimentally identified across the radioactive odd-A tin isotopes [24] together with their influence on the quadrupole moments. Excited states at high excitation energies in ^{131}Sn may also provide important information about core excitations and how they couple to a single neutron-hole to test the stability of the neutron shell closure [25]. They may also help identify single-particle states via feeding transitions.

The β decay of ^{131}In to excited states in ^{131}Sn is important for the overall understanding of the β-decay process in the neutron-rich region around $N = 82$, where the quenching of Gamow-Teller (GT) transition strength and the role of first-forbidden (FF) transitions is still controversial [26–28] and may impact neutron production in astrophysical scenarios [16].

β decay is a very powerful tool to exploit the population of a large range of excited states driven by the selection rules. In case of ^{131}In, where three long-lived β-decaying states are present, states with varying angular momenta in ^{131}Sn are populated. Furthermore, the feeding of high-lying states in the β decay of ^{131}In triggers the possibility of competing decay modes, including the emission of one neutron, but also the γ deexcitation. Apart from its interest from the point of view of nuclear structure [29–32], and the dependence on β-feeding states, the role of γ emission from neutron-unbound states has significant impact on neutron emission probabilities close to the driplines [17], which affects the r-process nucleosynthesis.

In this paper we present a detailed investigation of the structure of ^{131}Sn studied via the β decay of ^{131}In at the

ISOLDE facility at CERN and via mass measurements at the Ion Guide Isotope Separator On-Line (IGISOL) facility at the Accelerator Laboratory of the University of Jyväskylä. Three β-decaying indium states are known in ^{131}In. The $J^\pi = 9/2^+$ ground state ^{131g}In is dominated by the $\pi g_{9/2}^{-1}$ proton-hole configuration. The low-lying isomer ^{131m1}In is found at 376(3) keV [33], with $J^\pi = 1/2^-$, and can be related to the $\pi p_{1/2}^{-1}$ proton hole configuration. A higher-lying isomer, ^{131m2}In, is found at 3750(90) keV [33], or 3771(15) keV [34], for which a high angular momentum of $J^\pi = (21/2^+)$ is assumed. It can be identified as a member of the core-excited $\pi g_{9/2}^{-1} \nu h_{11/2}^{-1} f_{7/2}$ one-particle two-hole (1p2h) configuration [27].

Profiting from isomerically enhanced ion beams provided by the ISOLDE Resonance Ionization Laser Ion Source (RILIS) [35], the contributions from the decay from the three indium parent states have been isolated and the direct β feeding to the $3/2^+$ ground and $11/2^-$ isomeric states in ^{131}Sn measured. The discrepancies in the FF transition strengths reported in previous works [27,28] have been solved. The ^{131}Sn level scheme has been extended, and emission of γ rays above the neutron separation energy identified.

Furthermore, we provide excited-level lifetime measurements in ^{131}Sn to derive electromagnetic transition probabilities, for which the information is scarce. Transition rates shed light on the structure of excited states and probe nuclear models beyond what can be reached by spectroscopic information alone, since they are sensitive to the nuclear wave functions.

This paper is organized as follows. Information from literature about the excited structure of ^{131}Sn is summarized in Sec. II. The experimental methods and results for the IGISOL mass measurements are presented in Sec. III. Details about the experimental methods of the ISOLDE decay measurement are given in Sec. IV, while results on the excited structure of ^{131}Sn populated in β decay are presented in Sec. V. Excited-state lifetimes are addressed in Sec. VI. The results are then discussed in Sec. VII and conclusions are drawn in Sec. VIII.

II. PRIOR KNOWLEDGE OF THE STRUCTURE OF ^{131}Sn

The population of excited levels in ^{131}Sn through the β decay of ^{131}In was observed for the first time at OSIRIS by De Geer *et al.* [36], where the $\nu g_{7/2}^{-1}$ and $\nu s_{1/2}^{-1}$ neutron-hole states in ^{131}Sn were identified. Further studies performed at OSIRIS [27,37] expanded the ^{131}Sn level scheme notably, including the observation of the $\nu d_{5/2}^{-1}$ state and also the presence of a large number of core-excited states located around 4-MeV excitation energy. Levels populated in the β decay of the high-spin ^{131m2}In isomer were also identified, showing a strong resemblance to the decay of ^{132}In. The populated states deexcite in cascades with two or more γ rays down to the $11/2^-$ isomeric state of ^{131}Sn, which is associated to the $\nu h_{11/2}^{-1}$ configuration. No transition connecting the levels populated in the decay of ^{131m2}In with those assigned to the decay of either the ground state and/or first isomeric-state was observed, as expected from the large angular momentum difference between the ^{131m2}In and the others.

While spin and parities of the lowest-lying β-decaying $3/2^+$ ground state and $11/2^-$ isomeric state in ^{131}Sn have been measured by collinear laser spectroscopy [24], the energy of the $11/2^-$ state has not been precisely measured yet. The large spin difference with the $3/2^+$ ground state would require a slow M4 γ transition, which is not uncommon across the nuclear chart, but in this case the β-decay branch is dominant. In Ref. [27], the position of the state was determined by measuring the Q_β energy differences in the β decay of the ^{131}Sn isomers, yielding 69(14) keV. A more precise value of 65.1(5) keV was also proposed by Fogelberg *et al.* [27] based on the assignment of a 2369-keV $M2$ γ transition connecting the 2434-keV $\nu g_{7/2}^{-1}$ level to the $\nu h_{11/2}^{-1}$ isomer. This assignment has never been confirmed by $\gamma\gamma$ coincidences and still remains as a tentative value awaiting experimental confirmation.

Recently, the results of another β-decay study of ^{131}In performed at TRIUMF have been reported [28]. Expanded knowledge about excited states in ^{131}Sn, especially on the high-spin excited levels populated in the decay of ^{131m2}In, was provided. In addition, new measurements for the lifetimes of the indium β-decaying states were obtained, as well as a new half-life value for the 316(5) ns (23/2$^-$) isomer in ^{131}Sn.

The ^{131}Sn structure was also investigated at Argonne National Laboratory, where the excited levels were populated in the spontaneous fission of ^{248}Cm [38]. The study led to a better understanding of the yrast excitations in ^{131}Sn, providing also a rather complete interpretation of the high-spin states, in terms of 1p2h configurations.

Neutron transfer ^{130}Sn(d, p)^{131}Sn reactions [39] helped identifying the four lowest-lying neutron single-hole states in ^{131}Sn. Recently, neutron transfer reactions in inverse kinematics have been reported [40], including transfer on the 7^- isomer state in ^{130}Sn, leading to the population of high-lying 1p2h states in ^{131}Sn.

III. MASS MEASUREMENTS OF ^{131m}Sn

The excitation energy of the ^{131m}Sn isomeric state was measured at the IGISOL facility at the University of Jyväskylä, Finland [41,42]. Both the ground and isomeric states, were produced in proton-induced fission of a 15-mg/cm^2-thick ^{nat}U target using a 25-MeV proton beam with an average current of 1 μA. First, the fission products were stopped in a gas cell filled with helium at about 300 mbar. Then, they were extracted and guided through a sextupole ion guide [43]. Subsequently, a 30-kV acceleration potential was applied. The continuous beam was separated with respect to their mass-to-charge ratio $A/q = 131$ by a 55° dipole magnet and injected into the helium buffer gas-filled radio-frequency quadrupole cooler-buncher [44]. From there, the bunched beam was transported to the JYFLTRAP double Penning trap mass spectrometer [45].

In the first trap, the ions were cooled, purified, and centered using a mass-selective buffer gas cooling technique [46]. This step resulted in removing the majority of isobaric contaminants. Then the remaining ions were transferred to the second trap via a 1.5-mm-diameter diaphragm and, after about 600 μs, they were transferred back to the first trap for additional cooling. Finally, the singly charged ions were sent again to the
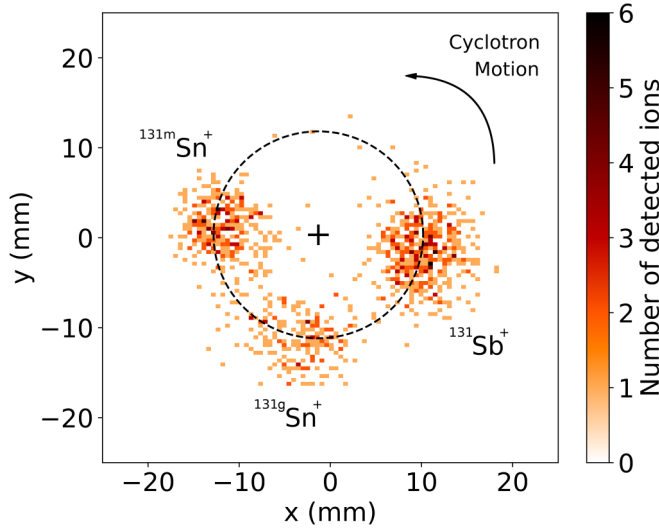
FIG. 1. Projection of the cyclotron motion of the ^{131g}Sn$^+$ and ^{131m}Sn$^+$ ions and their isobaric contaminant ^{131}Sb$^+$ onto the position-sensitive detector after a phase accumulation time of $t_{\text{acc}} = 575$ ms. The position of the center spot is indicated by the $+$ symbol. The average excitation radius is indicated with the dashed circle.

second trap. There the cyclotron frequency $\nu_c = qB/(2\pi m)$ in the magnetic field B was determined using the phase-imaging ion-cyclotron-resonance (PI-ICR) technique [47–49].

In the PI-ICR method, the cyclotron frequency is measured based on the phase difference between the cyclotron and magnetron motions of the ion after a phase accumulation time t_{acc}. In this work, four different t_{acc} values 485, 548, 575, and 713.2 ms, were applied. The final measurement was done with $t_{\text{acc}} = 575$ ms as it allowed us to resolve two long-lived states in ^{131}Sn, as well as the ^{131}Sb isobaric contaminant (see Fig. 1). The magnetic field B was determined by measuring the cyclotron frequency $\nu_{c,\text{gs}}$ of the ^{131g}Sn ground state.

From the frequency ratio between the singly charged ions of the ground and isomeric states, $r = \nu_{c,\text{gs}}/\nu_{c,m}$, the excitation energy of ^{131m}Sn, E_x, can be calculated as $E_x = (r - 1)[M_{\text{gs}} - m_e]c^2$, where $M_{\text{gs}} = 130.917053(4)$ u is the mass of the ^{131}Sn ground state taken from the Atomic Mass Evaluation 2020 [50], m_e is the mass of a free electron and c is the speed of light in vacuum.

Ground-state and isomer measurements ($\sim$29 and $\sim$10 min, respectively) were alternated to account for the fluctuations of the magnetic field. Due to limited statistics, the count rate was restricted to one detected ion per bunch to account for possible ion-ion interactions. This corresponds to up to three ions in a bunch considering a detector efficiency of about 30%. The systematic effects due to the temporal magnetic field fluctuation [$\delta B/B = 2.01(25) \times 10^{-12}$ min$^{-1} \times \delta t$, with δt being the time between the measurements], the magnetron phase advancement, and the angle error were included into the final uncertainty [51].

The frequency ratio measured in this work, $r = 1.000000525(15)$, corresponds to an excitation energy $E_x = 64.0(20)$ keV of the ^{131m}Sn $11/2^-$ isomeric state. This result provides the first direct measurement of the $11/2^-$ state excitation energy and is consistent with the literature [27] and
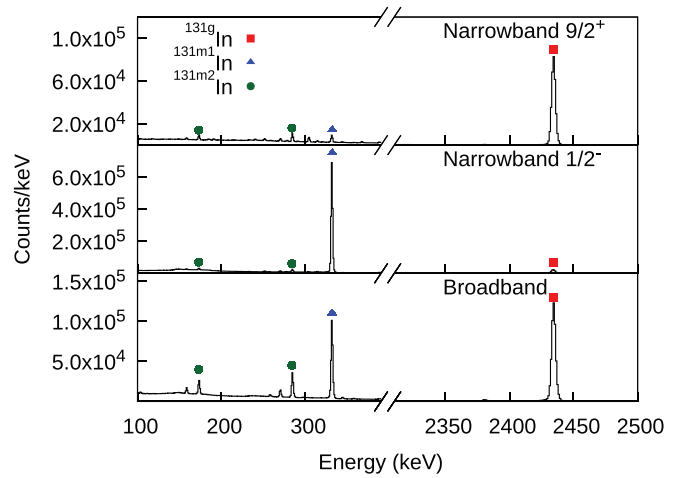

FIG. 2. Measured β-gated γ-ray energy spectra for the β decay of ^{131}In in three different ionization configurations. Top: RILIS lasers were set in narrow-band mode, with the optimal wavelength for the ionization of the ^{131g}In isomer. Center: Narrow-band mode with the optimal wavelength for the ionization of the ^{131m1}In isomer. Bottom: RILIS lasers were set in broadband mode, where maximum ionization efficiency was achieved and the strongest γ lines from ^{131m2}In were observed. A set of the most relevant γ rays emitted in the decay of the ^{131g}In, ^{131m1}In, and ^{131m2}In isomer states are marked.

with the results from γ-ray spectroscopy discussed later in this paper.

IV. β-DECAY SPECTROSCOPY MEASUREMENT AT ISOLDE

The excited structures in ^{131}Sn were populated via the β decay of the three ^{131}In β-decaying states. The experiment was carried out at the ISOLDE facility at CERN where indium isotopes were produced by the bombardment of a UC$_x$ target equipped with a neutron converter by 1.4-GeV protons from the CERN Proton Synchrotron Booster. Indium atoms thermally diffused out of the target and were ionized using RILIS [35]. The use of narrow-band lasers granted isomeric selectivity by exploiting of the difference in the hyperfine splitting of the isomeric and ground states [52]. Three different laser configurations were employed for the measurements. In two of them a narrow-band mode was used with a wavelength that enhanced the ionization of the ^{131g}In ($9/2^+$) and ^{131m1}In ($1/2^-$) β-decaying states, respectively, achieving a strong separation. The third configuration was a broadband wavelength mode where all three isomers were ionized at the same time, with an enhanced ionization efficiency. Figure 2 illustrates the high selectivity achieved in the experiment.

The indium ions were extracted by a 30-kV electrostatic potential, and then mass selected [53] and transported to the center of our detector setup at the ISOLDE Decay Station [54], where they were implanted on a movable aluminized mylar tape inside a T-shaped vacuum chamber. Four clover-type HPGe detectors were set up in a compact arrangement around the implantation point for γ-ray spectroscopy. The energy calibration was performed using standard sources and extended to 7.6 MeV by using neutron-capture γ-ray lines
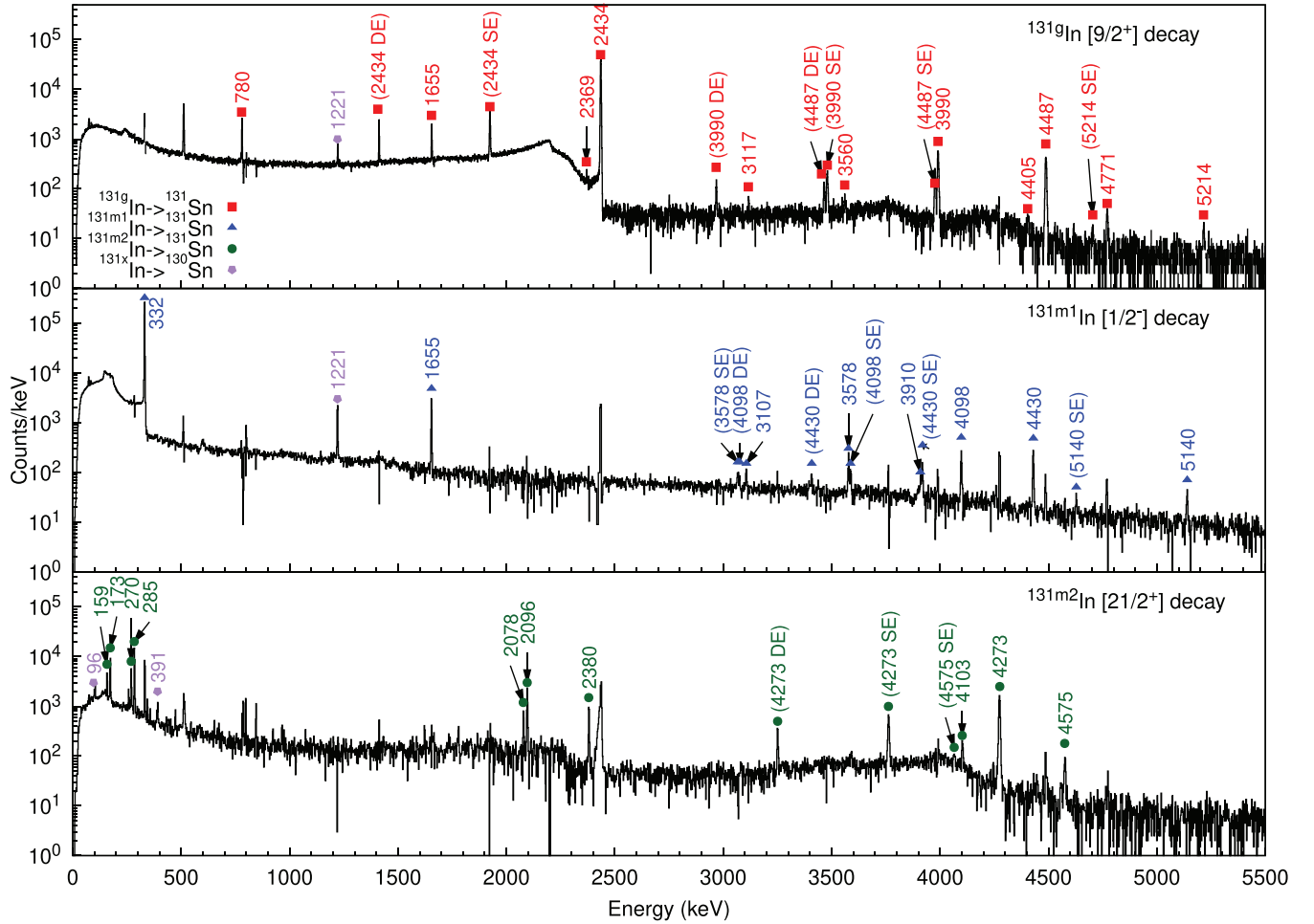
FIG. 3. Separated β-gated γ-ray spectra recorded for the decay of ^{131g}In (top), ^{131m1}In (middle), and ^{131m2}In (bottom). The three spectra have been generated from a linear combination of the spectra recorded with the three different RILIS laser configurations. The coefficients of the combination were selected in order to isolate the contributions of the decay from each β-decaying state. A set of the most relevant γ rays emitted in the decay of the ^{131g}In, ^{131m1}In, and ^{131m2}In isomer states are marked with the red squares, blue triangles, and green circles, respectively. Single-escape and full-escape peaks are labeled with SE and FE, respectively, along with their associated γ-ray energy.

induced in ^{56}Fe and ^{73}Ge by neutrons emitted from the target area during irradiation. Two LaBr$_3$(Ce) detectors, along with an ultrafast 3-mm-thick NE111A plastic scintillator used as a β detector were also employed for lifetime measurements of excited states using the advanced time-delayed $\beta\gamma\gamma(t)$ (fast timing) technique [55–57]. More details about the experiment can be found in Refs. [4,7,29,58,59].

The γ rays emitted in the β decay from the three ^{131g,131m1,131m2}In long-lived states can be unambiguously identified in our spectra by their distinctive time distribution, with half-lives of the order of 300 ms. The distinction is favored by the large difference between the short lifetime of the indium isomers in comparison with the longer half-lives of the daughter ^{131}Sn nucleus, 56.0(5) and 58.4(5) s for the $3/2^+$ and $11/2^-$ states, respectively [60].

V. EXCITED STRUCTURE OF ^{131}Sn

The identification of new transitions in ^{131}Sn was performed via the analysis of the singles, γ-γ, and β-gated spectra measured with different isomeric beam composition

provided by the RILIS ionization schemes discussed above. Figure 3 shows three spectra obtained for the decay of the ^{131}In beam corresponding to the narrow-band ($9/2^+$), narrow-band ($1/2^-$), and broadband laser configurations. The assignment of γ-ray transitions to the decay of the individual indium β-decaying states is done by comparing of the relative peak intensities for each resonant ionization configuration.

A. β decay of ^{131g}In

The γ-ray spectra measured in our experiment shows high-energy transitions up to 7 MeV, see Fig. 4. These lines appear in the β-gated spectra, with a time distribution compatible with the decay of indium. The γ transitions observed in the decay of ^{131g}In ground state are listed in Table I. High-energy γ rays are reported in Ref. [28], but without assignment to the decay of any specific isomer. Thanks to the isomer selectivity provided by RILIS, we were able to confirm that almost all of them exclusively belong to the decay of the ^{131g}In, in spite of having the smallest β-decay energy window. The assignment is supported by their observed enhanced intensity

TABLE I. Observed excited states in ^{131}Sn and γ-ray intensities measured in the decay of the three ^{131}In β-decaying states. See text for details.

E_i (keV)	J_i^π	E_f (keV)	J_f^π	E_γ (keV)	I_γ^a (%) [^{131g}In]	I_γ^b (%) [^{131m1}In]	I_γ^c (%) [^{131m2}In]
0	$3/2^+$						
65.4(7)	$11/2^-$						
331.6(3)	$(1/2^+)$	0.0	$3/2^+$	331.6(3)	–	100	–
1654.7(4)	$(5/2^+)$	0.0	$3/2^+$	1654.7(4)	2.4(4)	3.7(4)	–
2434.1(5)	$(7/2^+)$	0.0	$3/2^+$	2434.1(5)	100	–	–
		65.4(7)	$11/2^-$	2368.7(5)	0.20(4)	–	–
		1654.7(6)	$(5/2^+)$	779.6(4)	2.2(4)	–	–
3438.4(4)	$(3/2^-)$	331.6(3)	$(1/2^+)$	3106.8(4)	–	0.20(4)	–
		0.0	$3/2^+$	3439.0(13)	–	0.06(2)	–
3910.0(3)	$(1/2,3/2)$	331.6(3)	$(1/2^+)$	3578.4(3)	–	0.65(8)	–
		0.0	$3/2^+$	3910.6(8)	–	0.16(4)	–
3989.6(5)	$(7/2^+)$	0.0	$3/2^+$	3989.6(6)	3.7(6)	–	–
		1654.7(6)	$(5/2^+)$	2335.9(7)	0.12(3)	–	–
		2434.1(5)	$(7/2^+)$	1555.4(5)	0.15(4)	–	–
4168.1(9)	$(15/2^-)$	65.4(7)	$11/2^-$	4102.7(6)	–	–	11(2)
4259.1(9)		0.0	$3/2^+$	4259.1(9)	0.15(4)	–	–
4311.6(8)	$(15/2^+)$	65.4(7)	$11/2^-$	4245.6(5)	–	–	3.2(6)
4339.3(7)	$(17/2^+)$	65.4(7)	$11/2^-$	4273.3(3)	–	–	100
		4168.1(9)	$(15/2^-)$	171.2(3)	–	–	1.2(3)[d]
4352.4(10)		0.0	$3/2^+$	4352.4(10)	0.06(3)	–	–
4404.5(5)	$(7/2^+)$	0.0	$3/2^+$	4404.6(7)	0.15(4)	–	–
		1654.7(6)	$(5/2^+)$	2750.6(7)	0.08(2)	–	–
		2434.1(5)	$(7/2^+)$	1969.4(7)	0.08(2)	–	–
4429.6(3)	$(1/2,3/2)$	0.0	$3/2^+$	4429.8(3)	–	1.2(2)	–
		331.6(3)	$(1/2^+)$	4097.9(4)	–	0.8(1)	–
4486.8(6)	$(7/2^+)$	0.0	$3/2^+$	4486.7(6)	3.6(7)	–	–
		1654.7(6)	$(5/2^+)$	2833.8(6)	0.19(4)	–	–
		2434.1(5)	$(7/2^+)$	2053.0(5)	0.10(2)	–	–
4487.2(15)	$(15/2^+)$	65.4(7)	$11/2^-$	4421.5(13)	–	–	0.5(2)
4512.6(7)	$(19/2^-)$	65.4(7)	$11/2^-$	4446.8(5)	–	–	2.7(5)
		4168.1(9)	$(15/2^-)$	344.4(2)	–	–	6.6(8)
		4339.3(7)	$(17/2^+)$	173.4(2)	–	–	42(5)
4576.3(9)	$(17/2^-)$	4168.1(9)	$(15/2^-)$	408.2(4)	–	–	0.36(11)
4623.9(7)	$(19/2^+)$	4339.3(7)	$(17/2^+)$	284.6(2)	–	–	43(5)
4641.1(7)	$(17/2^+)$	65.4(7)	$11/2^-$	4574.7(6)	–	–	4(1)[d]
		4168.1(9)	$(15/2^-)$	473.4(2)	–	–	1.8(3)
		4311.6(8)	$(15/2^+)$	329.6(3)	–	–	3.6(10)[d]
		4339.3(7)	$(17/2^+)$	302.0(3)	–	–	0.7(2)[d]
		4487.2(15)	$(15/2^+)$	153.3(5)	–	–	0.7(4)[d]
4671.2(7)	$(23/2^-)$	4512.6(7)	$(19/2^-)$	158.7(2)	–	–	28(3)
4712.6(5)	$(1/2,3/2)$	0.0	$3/2^+$	4712.6(5)	–	0.11(3)[d]	–
4770.7(7)	$(21/2^-)$	4512.6(7)	$(19/2^-)$	258.2(2)	–	–	3.2(4)
		4671.2(7)	$(23/2^-)$	99.7(3)	–	–	1.9(2)
4771.1(7)		0.0	$3/2^+$	4770.9(7)	0.28(6)	–	–
		1654.7(6)	$(5/2^+)$	3116.8(7)	0.12(3)	–	–
4774.7(8)	$(25/2^-)$	4671.2(7)	$(23/2^-)$	103.6(2)	–	–	2.4(3)
4810.3(8)		4512.6(7)	$(19/2^-)$	297.8(3)	–	–	1.0(2)
4900.7(8)		4512.6(7)	$(19/2^-)$	388.2(3)	–	–	1.7(2)
4941.2(8)		4671.2(7)	$(23/2^-)$	270.2(2)	–	–	14(2)
		4770.7(7)	$(21/2^-)$	168.3(3)	–	–	<2[d]
5055.8(7)	$(21/2^+)$	4623.9(7)	$(19/2^+)$	432.0(3)	–	–	0.8(2)
		4512.6(7)	$(19/2^-)$	543.3(3)	–	–	0.82(14)
5058.3(7)		4512.6(7)	$(19/2^-)$	545.9(3)	–	–	1.0(2)
		4770.7(7)	$(21/2^-)$	287.4(5)	–	–	0.7(4)[d]
5110.3(9)		2434.1(5)	$(7/2^+)$	2676.2(8)	0.08(4)	–	–
5120.0(8)		4623.9(7)	$(19/2^+)$	496.2(3)	–	–	1.2(2)
5139.9(4)	$(1/2,3/2)$	0.0	$3/2^+$	5139.9(4)	–	0.21(4)[d]	–

TABLE I. (*Continued.*)

E_i (keV)	J_i^π	E_f (keV)	J_f^π	E_γ (keV)	I_γ [a] (%) [^{131g}In]	I_γ [b] (%) [^{131m1}In]	I_γ [c] (%) [^{131m2}In]
5214.3(6)		0.0	$3/2^+$	5214.0(8)	0.19(5)	–	–
		1654.7(6)	$(5/2^+)$	3560.0(7)	0.12(3)	–	–
5286.6(8)		4770.7(7)	$(21/2^-)$	515.9(4)	–	–	4.5(10)
5297.9(8)		4623.9(7)	$(19/2^+)$	674.0(2)	–	–	1.4(2)
5393.4(8)		4671.2(7)	$(17/2^+)$	722.2(3)	–	–	0.64(10)
5412.7(10)		0.0	$3/2^+$	5412.7(10)	0.07(3)	–	–
		2434.1(5)	$(7/2^+)$	2978.4(5)	<0.1	–	–
5594.7(12)		1654.7(6)	$(5/2^+)$	3940.1(11)	0.12(3)[d]	–	–
5595.0(7)		4671.2(7)	$(23/2^-)$	923.9(3)	–	–	1.3(2)
		4774.7(8)	$(25/2^-)$	820.4(3)	–	–	0.66(10)
		4941.2(8)		653.6(2)	–	–	1.17(15)
5608.9(7)		4512.6(7)	$(19/2^-)$	1096.3(3)	–	–	0.96(14)
5644.5(7)		4671.2(7)	$(23/2^-)$	973.8(2)	–	–	1.3(2)
		5268.6(6)		357.2(3)	–	–	1.1(2)
5646.6(11)		0.0	$3/2^+$	5646.5(11)	0.07(2)[e]	–	–
		1654.7(6)	$(5/2^+)$	3993.5(7)	0.004(2)[e]	–	–
5739.6(8)		4774.7(8)	$(25/2^-)$	964.8(2)	–	–	2.7(3)
6175.2(8)		4512.6(7)	$(19/2^-)$	1662.4(3)	–	–	0.5(2)[d]
6193.6(8)+Y		Y		6193.6(8)	0.026(6)[e]	–	
6246.0(8)		4623.9(7)	$(19/2^+)$	1622.0(2)	–	–	3.0(4)
6321.7(9)+Y		Y		6321.7(9)	0.041(10)[e]	–	–
6332.1(8)		4512.6(7)	$(19/2^-)$	1819.3(3)	–	–	0.6(2)[d]
6345.8(7)+Y		Y		6345.8(7)	0.12(2)[e]	–	–
6457.0(7)+Y		Y		6457.0(8)	0.065(14)[e]	–	–
6557.3(7)+Y		Y		6557.3(7)	0.12(2)[e]	–	–
6559.2(8)		5297.9(8)		1261.2(4)	–	–	0.48(9)
6591.2(8)+Y		Y		6591.2(8)	0.024(7)[e]	–	–
6694.1(8)+Y		Y		6694.1(8)	0.035(8)[e]	–	–
6709.4(8)		4623.9(7)	$(19/2^+)$	2085.3(4)	–	–	1.5(2)
6720.0(7)	$(21/2^+)$	4339.3(7)	$(17/2^+)$	2380.4(3)	–	–	17(2)
		4512.6(7)	$(19/2^-)$	2207.4(3)	–	–	2.4(3)
		4623.9(7)	$(19/2^+)$	2095.9(2)	–	–	32(4)
		4641.1(7)	$(17/2^+)$	2078.3(3)	–	–	10.0(12)
		4770.7(7)	$(21/2^-)$	1949.7(4)	–	–	0.7(3)
		4900.7(8)		1818.5(6)	–	–	1.0(4)
		4941.2(8)		1778.6(3)	–	–	2.9(4)
		5286.6(6)		1432.9(3)	–	–	1.5(2)
		5297.9(8)		1422.3(4)	–	–	0.6(2)
		5608.9(7)		1111.3(3)	–	–	0.9(2)
6743.3(8)+Y		Y		6743.3(8)	0.08(2)[e]	–	–
6800.0(8)+Y		Y		6800.0(8)	0.058(14)[e]	–	–
6806.0(11)+Y		Y		6806.0(11)	0.028(9)[e]	–	–
6923.0(8)		4623.9(7)	$(19/2^+)$	2298.8(3)	–	–	0.44(7)
6936.5(11)		65.4(7)	$11/2^-$	6870.2(8)	0.068(14)[e]	–	–
		2434.1(5)	$(7/2^+)$	4503.2(8)	0.07(4)[d]	–	–
6955.5(9)		4623.9(7)	$(19/2^+)$	2331.4(5)	–	–	0.73(13)
7003.3(10)+Y		Y		7003.3(10)	0.023(8)[e]	–	–
7053.2(8)	$(21/2^+)$	4623.9(7)	$(19/2^+)$	2429.4(3)	–	–	4.0(7)[d]
		4671.2(7)	$(23/2^-)$	2381.2(8)	–	–	0.3(2)[d]
7090.9(11)+Y		Y		7090.9(11)	0.028(10)[e]	–	–

[a]Relative γ intensities normalized to 100 units for the 2434-keV $7/2^+ \to 3/2^+$ transition. For intensity per 100 decays of the parent ^{131g}In multiply by 0.65(11).

[b]Relative γ intensities normalized to 100 units for the 332-keV $1/2^+ \to 3/2^-$ transition. For intensity per 100 decays of the parent ^{131m1}In multiply by 0.42(12).

[c]Relative γ intensities normalized to 100 units for the 4273-keV $17/2^+ \to 11/2^-$ transition. For intensity per 100 decays of the parent ^{131m2}In multiply by 0.75(6).

[d]Intensity derived from $\gamma\gamma$ coincidences.

[e]Intensity derived from β-gated spectrum.
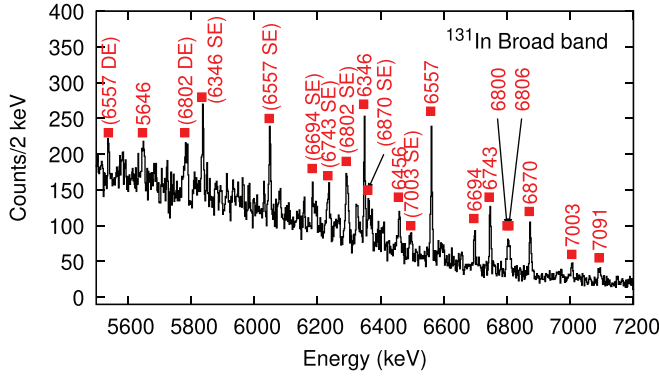
FIG. 4. β-gated high-energy spectrum measured in broadband RILIS mode for the ^{131}In decay. All of the γ lines were assigned to the decay of ^{131g}In.

in the narrow-band $(9/2^+)$ spectra, while they are missing in the narrow-band $(1/2^-)$ data. This result discards their assignment to the ^{131m1}In decay but also to ^{131m2}In, whose contribution is similar in both narrow-band modes (see Fig. 2). In addition, no $\gamma\gamma$ coincidences have been observed, inhibiting their assignment to the ^{131m2}In decay, where decay by several γ transitions should be expected given the high spin of the $(21/2^+)$ parent state and the low spin of low-lying ^{131}Sn states. It should be mentioned that a certain inconsistency has emerged between the energies of the high-energy γ rays reported in Ref. [28] and those measured in this work. Only a few γ rays observed in our spectra were identified with those reported in Ref. [28], displaying a systematic difference in energy of around $\sim$4 keV. In the present work, the energy calibration up to 7.6 MeV was cross-checked using neutron-capture γ rays observed in the same data during measurement.

The location of the high-energy γ rays in the level scheme is uncertain. The absence of $\gamma\gamma$ coincidences indicates that the levels depopulated by these transitions are directly fed in β decay. Those levels would deexcite to either the $3/2^+$ ground state or the $11/2^-$ β-decaying isomers in ^{131}Sn. The β-decay selection rules for "allowed" decays from the $9/2^+$ ground state constrain the population of states in the daughter nucleus to $7/2^+$, $9/2^+$, and $11/2^+$. Of those possibilities, only the levels with $J^\pi = 7/2^+$ would have a preferred decay branch to the $3/2^+$ ground state by an $E2$ γ transition, whereas the $9/2^+$ and $11/2^+$ levels would decay predominantly to the $11/2^-$ isomer by $E1$ transitions. Taking this into consideration, one can assume that most of the transitions feed the $11/2^-$ isomer, but the lack of confirmation by $\gamma\gamma$ coincidences does not allow us to rule out either of the two possibilities. We have included the high-energy γ rays in the level-scheme (see Fig. 5) deexciting levels whose energy has been labeled as $E_\gamma + Y$, where Y denotes either 0 or 65.4 keV (the energy of the $11/2^-$ isomer) but not necessarily the same for all levels.

The direct feeding of ^{131}Sn and ^{130}Sn ground states, was estimated from the balance between the γ-ray feeding and the total decay intensity of each tin isotope. In the case of ^{131g}In decay, it is possible to populate both β-decaying states in ^{131}Sn, as well as the 0^+ and (7^-) β-decaying states in ^{130}Sn (see Fig. 5). The total number of decays for each branch was

derived from the γ-ray intensities. However, previous studies on ^{131}Sn did not disentangle the decay of the two β-decaying states. Hence, the absolute intensities for the γ rays from ^{131}Sn $3/2^+$ and $11/2^-$ states have been obtained from our data. In particular, the absolute intensity for ^{131}Sn $3/2^+$ decay was taken from our ^{131m1}In decay data, while the intensities from ^{131}Sn $11/2^-$ have been measured from the ^{132}In (7^-) decay. For the β-n branch, the absolute γ-ray intensities for both the 0^+ and 7^- states have been taken from Ref. [61].

Our analysis yields a negligible population of the ^{131}Sn $3/2^+$ and the ^{130}Sn 0^+ levels, as expected due to the spin difference from the ^{131g}In $(9/2^+)$ initial state. The $11/2^-$ level receives 25(6)% of the total feeding, in contrast to the $5(^{+15}_{-5})\%$ β feeding reported in Ref. [28]. The reason is that an important part of the $11/2^-$ state feeding was erroneously assigned to ground-state feeding in the β decay of ^{131m1}In in Ref. [28] (see Sec. V B), resulting in a reduced apparent feeding to the $11/2^-$ state. Our new value for the β feeding yields a $\log ft$ of 5.49(11) for the first-forbidden $\nu h_{11/2} \rightarrow \pi g_{9/2}$ transition, which is now compatible with the two other FF transitions measured in the ^{131m1}In decay.

We have investigated the population of the excited levels in ^{130}Sn via β-delayed neutron emission from ^{131}In. Compared to earlier works, owing to isomer selectivity, in our study it was possible to obtain β-n branches for each isomer separately. Based on the estimated ground-state feedings discussed above, we have calculated a $P_n = 2.4(6)\%$ value for the ^{131g}In decay. The γ-ray intensities in ^{130}Sn populated by the β-delayed neutron branch are compiled in Table II for the three β-decaying ^{131}In isomers.

B. β decay of ^{131m1}In

The γ transitions observed in ^{131m1}In are listed in Table I, and the extended level scheme is shown in Fig. 6. Estimation of the direct ground state feeding in both β and βn branches was done using the measured γ-ray intensities from the β decay of ^{131}Sn and ^{130}Sn daughters. The apparent β feeding of the ^{131}Sn $3/2^+$ ground state was estimated to be 54(7)%, while that of the 332-keV $(1/2^+)$ level yielded 42(7)%. These results differ from those reported in Refs. [27,28] because in previous works an important fraction of the $\nu h_{11/2} \rightarrow \pi g_{9/2}$ transition intensity in ^{131g}In decay was misassigned to the ground state feeding in the ^{131m1}In β decay. This limitation was overcome in the present work thanks to the RILIS isomer selectivity.

Two similar $\log ft$ values of 5.37(6) and 5.41(8) were calculated for the $3/2^+$ and $(1/2^+)$ states, respectively. These values are consistent with the expected FF character of the transitions. An apparent direct β feeding to the $(5/2^+)$ $\nu d_{5/2}^{-1}$ and $3/2^-$ $\nu(dh^{-2})f_{3/2}$ single-particle/hole states at 1665 and 3438 keV is also observed. In addition, directly fed higher-lying levels are observed, including two newly proposed at 4713 and 5140 keV. It is worth noting that the state at 4045(4) keV identified as $1/2^-$ in Refs. [2,39], which can be expected to be populated by an allowed β-decay branch has not been observed, see Fig. 3.

The γ-ray intensities observed from the β-n branch are presented Table II. In the decay of ^{131m1}In, the most intense γ
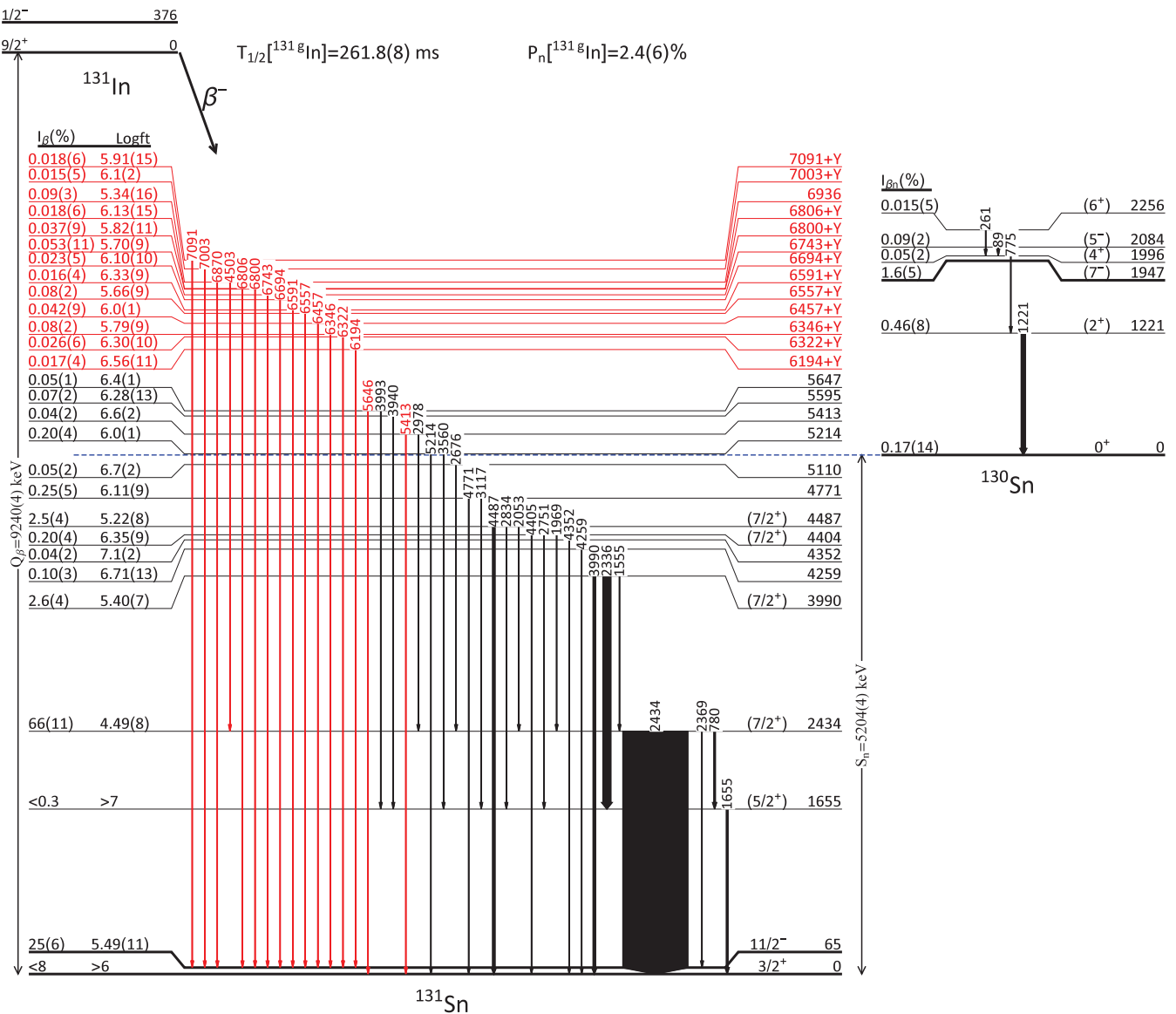
FIG. 5. Level scheme of ^{131}Sn and ^{130}Sn observed following the β decay of the ^{131g}In $(9/2^+)$ β-decaying state. Levels and transitions previously identified are colored in black, while those newly identified in this work are highlighted in red. The states populated in ^{130}Sn via β-delayed neutron emission are depicted at the right-hand side.

ray from the β-n branch observed was at 1221 keV, which corresponds to the decay of the first excited (2^+) state in ^{130}Sn. In addition, the population of the levels at 1995 (4^+), 2028 (2^+), and 2492 keV $(3^-, 4^+)$ is confirmed by $\gamma\gamma$ coincidences of the 1271-keV γ ray with the 1221-keV transition. Population to higher-spin levels in ^{130}Sn has not been observed in this case. Taking into account the measured ground state feeding, the β-delayed one neutron emission probability was estimated to be $P_n = 1.2(6)\%$.

C. β decay of ^{131m2}In

A complete isomeric separation was not possible for the ^{131m2}In $(21/2^+)$ β-decaying state but, given the large difference between the parent spin and those of the other two β-decaying states, it was possible to unambiguously identify

transitions via $\gamma\gamma$ coincidences and the comparison of the relative intensities between the different laser configurations. The β decay populates states high-spin states and, therefore, their deexcitation occurs mostly by cascades of two or more γ rays towards the $11/2^-$ isomer in ^{131}Sn. Given the large spin difference, it is very unlikely to populate the same states as in the decay of the other two β-decaying ^{131}In states, with the exception of the $11/2^-$ level. The level scheme is shown in Fig. 7, while the corresponding γ-ray transitions energies and intensities are listed in Table I.

Due to the large number of low-energy γ rays, internal conversion has a non-negligible influence on transition intensities and, thus, the apparent β feedings. The total conversion coefficients were calculated using Bricc [62] assuming the most likely multipolarities.

TABLE II. Observed excited states in ^{130}Sn and γ-ray intensities measured in the decay of the three ^{131}In β-decaying states. See text for details.

E_i (keV)	J_i^π	E_f (keV)	J_f^π	E_γ (keV)	I_γ[a] (%) [^{131g}In]	I_γ[b] (%) [^{131m1}In]	I_γ[c] (%) [^{131m2}In]
0	0^+						
1221.4(6)	(2^+)	0	0^+	1221.6(6)	0.89(13)	3.0(2)	–
1994.8(12)	(4^+)	1221.4(6)	(2^+)	773.5(6)	0.17(3)	0.06(3)	–
2028.3(5)	(4^+)	0	0^+	2028.3(6)	–	0.12(3)	–
		1221.4(6)	(2^+)	807.0(6)	–	0.08(2)	–
2084.6(15)	(5^-)	1994.8(12)	(4^+)	90.0(12)	0.057(12)	–	–
2256.1(13)	(6^+)	1994.8(12)	(4^+)	261.0(12)	0.023(8)	–	–
2338.5(7)	(8^+)	1946.88(10)	(7^-)	391.4(6)	–	–	11.7(13)
2434.9(13)	(10^+)	2338.5(7)	(8^+)	96.4(8)	–	–	6.2(7)
2492.5(10)	$(3^-, 4^+)$	1221.4(6)	2^+	1271.0(5)	–	0.04(2)	–

[a,b,c]Relative intensity normalization employed (same as in Table I).

The ^{131m2}In $(21/2^+)$ β decay largely feed states with dominant 1p2h neutron configurations, which correspond to the core excited states in ^{132}Sn populated from ^{132}In [4] with an extra coupling to a $\nu h_{11/2}^{-1}$ neutron hole. All of the previously observed positive- and negative-parity states are confirmed, with the exception of the $(13/2^+)$ level at 4285 keV observed in Ref. [40], in a transfer reaction on the (7^-) isomeric component of a ^{130}Sn beam. The 4671- and 4941-keV states are the most strongly β fed among those observed in transfer reaction. New levels and γ-decay branches are observed for the first time following the β decay (see Fig. 7), including those feeding the isomeric $(23/2^-)$ 4671-keV state [25].

Intensities are listed in Table II. The population of levels in ^{130}Sn via β-delayed neutron emission is also possible in the decay of ^{131m2}In, as indicated by the observation of γ rays from high-spin states in ^{130}Sn. The P_n values can be extracted from the decay activities from the ^{131m1}Sn $11/2^-$ and ^{130m1}Sn (7^-) isomeric states. By comparing the relative γ-ray intensities $P_n = 7(4)\%$ is derived. No direct or indirecct population of the ^{131}Sn $3/2^+$ state and the ^{130}Sn 0^+ state was assumed, based on the high $(21/2^+)$ spin of ^{131m2}In. A more precise value can be obtained if direct β feeding of the ^{131}Sn $11/2^-$ and the ^{130}Sn (7^-) isomeric states is assumed to be negligible. In this case the ^{131m2}In intensity can be obtained directly from the intensity of the γ rays belonging to ^{131}Sn. Using this approach, $P_n = 8.9(8)\%$ is calculated, in agreement with the $7(4)\%$ derived from the daughter activities.
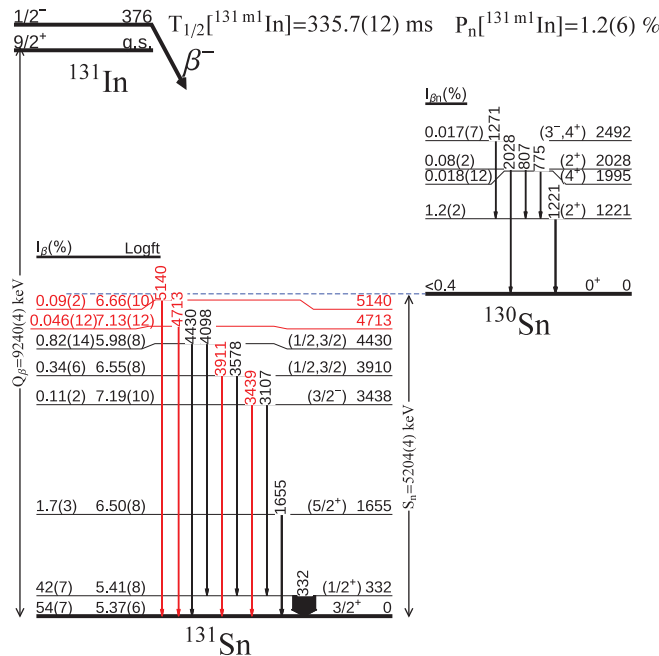
D. Half-lives of the ^{131}In β-decaying states

The lifetimes of all three ^{131}In β-decaying states have been measured by analyzing the time distribution of events with respect to the time of proton impact on the production target. For this analysis we have used the events recorded in the HPGe clover detectors with no extra condition. The contribution of the Compton background under full-energy peaks has been subtracted. The events have been selected by using the narrow-band RILIS data set when available and by choosing the strongest γ rays emitted after the decay of each of the three states. The choice of γ rays in itself grants a high selectivity of the isomer under study, since we do not observe states in ^{131}Sn populated in the decay of more than one long-lived state, neither directly nor indirectly; see Table I.

The time distributions were fitted to a single exponential plus a constant component. To account for dead-time effects due to the high count rate at the beginning of the decay window, the lower end of the fit range was probed with a χ^2 test to verify the expected exponential behavior [59]. In Fig. 8, the decay curves of the most intense γ rays considered in this analysis for each β-decaying state are depicted. The time distribution for each selected γ-ray transition was fitted independently.
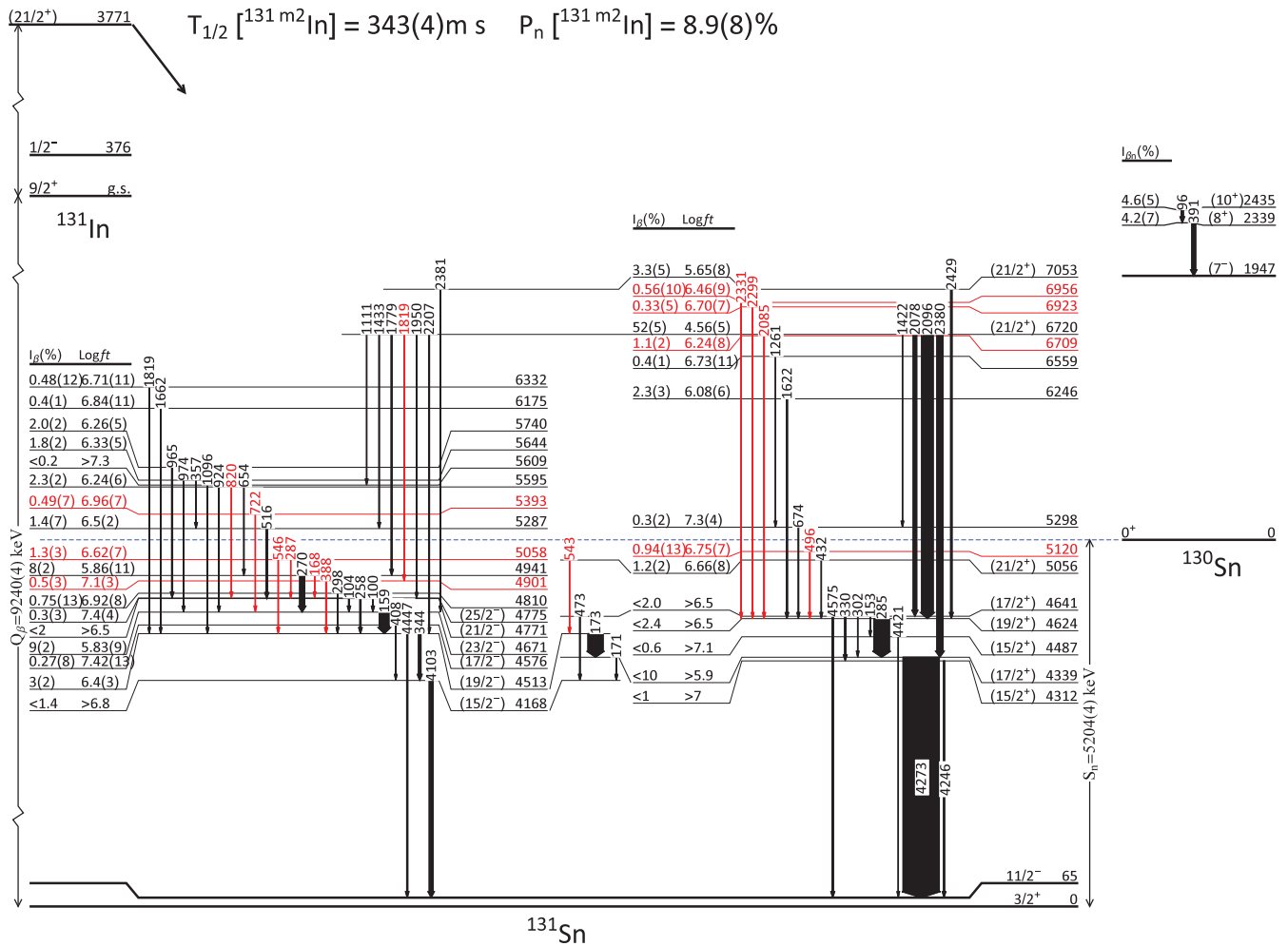

FIG. 6. Level scheme of ^{131}Sn observed in the β decay of ^{131m1}In $(1/2^-)$. The two new levels and four new γ transitions identified in this work for this decay are highlighted in red. The β-n branch populating excited states in ^{130}Sn is shown on the right-hand side.

FIG. 7. Level scheme of ^{131}Sn observed following the β decay of the ^{131m2}In ($21/2^+$) β-decaying state. Levels and transitions previously identified are in black, while those newly identified in this work are highlighted in red.

New lifetime values for the three β-decaying states in ^{131}In were obtained from the weighted average of the results of the individual fits to the time distributions. Note that only statistical uncertainties are included. The results are compiled in Table III and compared to those existing in the literature [28,60,63]. The agreement is very good, although our results have much higher statistical precision. Our results yield a slightly longer half-life for the ^{131m2}In state than for the ^{131m1}In one.

TABLE III. Measured half-life values for the three ^{131}In β-decaying states. It should be noted that the values quoted in the last column correspond with measurements without isomer selectivity.

$T_{1/2}$ ms State	This work	Fogelberg *et al.* [27]	Dunlop *et al.* [28]	Other values
^{131g}In	261.8(8)	280(30)	265(8)	261(3) [63] 278(7) [64]
^{131m1}In	335.7(12)	350(50)	328(15)	
^{131m2}In	343(4)	320(60)	323(55)	

VI. LIFETIMES OF EXCITED STATES IN ^{131}Sn

The information available prior to this work regarding the lifetimes of the excited levels in ^{131}Sn was scarce, since only a value of $T_{1/2} = 316(5)$ ns for the high-spin ($23/2^-$) 4671-keV isomer has been reported [25,28]. Lifetimes of excited states down to the 10-ps range have been investigated in this work by means of the advanced time-delayed (ATD) fast-timing method [55–57]. The measurements were performed in triple coincidences with the time differences taken between the fast β and LaBr$_3$(Ce) detectors together with an additional γ-ray energy gate on the HPGe detectors. The use of two LaBr$_3$(Ce) detectors made it possible to perform two independent measurements for the same lifetime, one per each β-LaBr$_3$(Ce) combination. In addition, $\gamma\gamma$(t) time differences between the two LaBr$_3$(Ce) detectors were used when possible. The analysis procedure is similar to that described in Refs. [4,7,59].

A. The l-forbidden $\nu 3s_{1/2}^{-1} \rightarrow \nu 2d_{3/2}^{-1}$ $M1$ transition

Lifetimes of single-particle states are important for the shell-model interpretation of the nuclear structure. In our
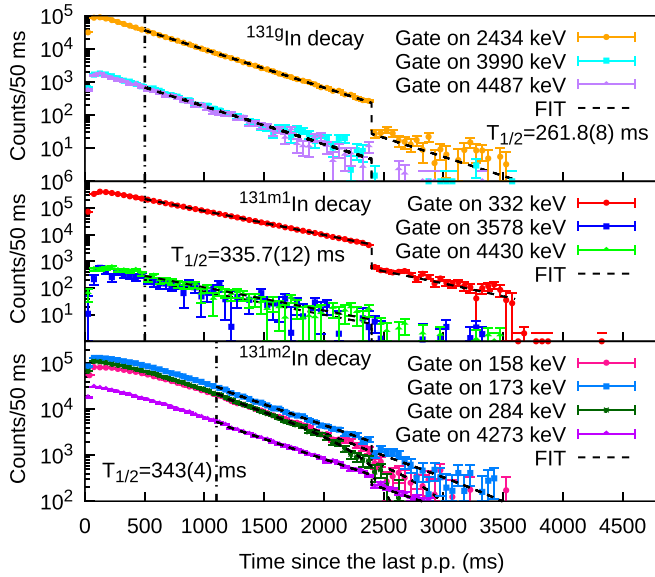
FIG. 8. Time distribution analysis of the ^{131g}In, ^{131m1}In, and ^{131m2}In lifetimes. Time distributions relative to the arrival of the last proton pulse and exponential decay fit curves. The steplike structure is due to the pulsed structure of protons impinging on the production target. The vertical dot-dashed line represents the starting point of the fitting range. This value was probed to avoid influence of dead time.

study, the lifetime of the 332-keV $(1/2^+)$ level in ^{131}Sn provides a direct measurement of the electromagnetic transition strength between the $\nu 3s_{1/2}^{-1}$ and the $\nu 3d_{3/2}^{-1}$ single-particle states. In the extreme shell model, the magnetic dipole transition between them would be a strictly l-forbidden transition due to the $\Delta l = 2$ change required [65]. The breaking of the $\Delta l = 0$ rule is not uncommon along the nuclear chart, being understood as a phenomena arising from configuration mixing [66,67].

The 332-keV level is populated in the decay of the ^{131m1}In $(1/2^-)$ isomer. However, it is almost entirely fed by direct β feeding and thus the analysis was performed using $\beta\gamma(t)$ fast-timing events. The β-gated γ-ray spectra registered in both LaBr$_3$(Ce) and HPGe detectors, employing for the broadband laser configuration are depicted in Fig. 9. The 2434-keV transition was employed as a reference for the prompt time response. The assumption of the prompt behavior of this transition is consistent with the assumed $E2$ $\nu g_{7/2}^{-1} \to d_{3/2}^{-1}$ single-particle transition, leading to a low collective $B(E2)$ value of around 1 W.u., which translates into a lifetime of $\sim$0.2 ps for this level, below the sensitivity of the technique. Since the transition is only observed in the decay of ^{131g}In, it was verified that the time response of the β detector is the same for the ^{131g}In and ^{131m1}In decays. The centroid shift analysis for one of the β-LaBr$_3$(Ce) combinations is illustrated in Fig. 9. The contribution of the Compton background has been subtracted from the peak time distribution.

We have adopted the weighted average of four independent measurements, $\tau = 21(5)$, 27(5), 39(8), and 19(8) ps. We use the external uncertainty, that takes into account the value dispersion and, for further safety margin, we impose a
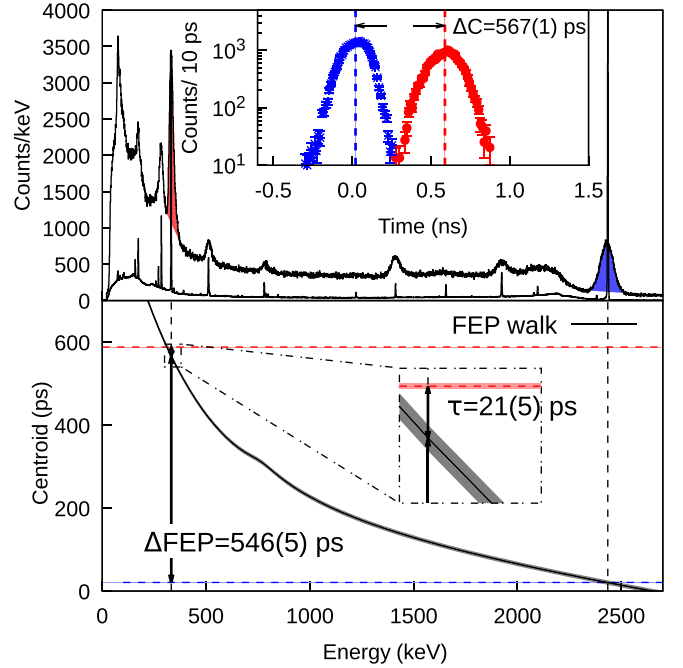

FIG. 9. Top: β-gated γ-ray spectra for the LaBr$_3$(Ce) and HPGe detectors. The inset shows the fast-timing $\beta\gamma(t)$ distributions for the 332- (red) and 2434-keV (blue) transitions for a specific combination using a LaBr$_3$(Ce) detector. The corresponding contribution from the Compton background has been estimated and subtracted. The lifetime of the 332-keV $(1/2^+)$ state was derived by the centroid shift method using the 2434-keV transition as a prompt reference. Bottom: Calibrated full energy peak (FEP) prompt curve, derived from calibration sources. The inset depicts the comparison between the shift of the two distributions (ΔC) and the shift in the FEP curve (ΔFEP) between the 2434- and 332-keV energies.

coverage of 1.4 standard deviation (σ) to account for the 1.4 σ difference between the maximum and minimum values. A final value of $\tau = 26(6)$ ps [$T_{1/2} = 18(4)$ ps] for the 332-keV state was obtained, from which the reduced transition probabilities for the 332-keV transition was derived. Assuming a pure $M1$ character, the half-life yields a $B(M1) = 0.059(12)$ μ_N^2 [0.033(7) W.u.]. On the other hand, by assuming a pure $E2$ multipolarity a very unrealistic $B(E2) = 8(2) \times 10^3$ e^2 fm^4 [195(42) W.u.] value is obtained. These values should be understood as upper limits, since the $M1/E2$ mixing ratio for the 332-keV transition is unknown but, in view of the $B(E2)$ rate, the $E2$ branch should be negligible.

B. Lifetimes of core-excited states

In the ^{131m2}In isomer decay, only core-excited levels with high spin are directly populated, due to the high $(21/2^+)$ spin of the β-decaying state. The large difference in angular momentum between these states and the $11/2^-$ isomer in ^{131}Sn favors deexciting γ-ray cascades. This situation is favorable for studying level lifetimes via the ATD $\beta\gamma\gamma(t)$ and $\gamma\gamma(t)$ methods. Lifetimes of several high-energy states have been measured in this work.
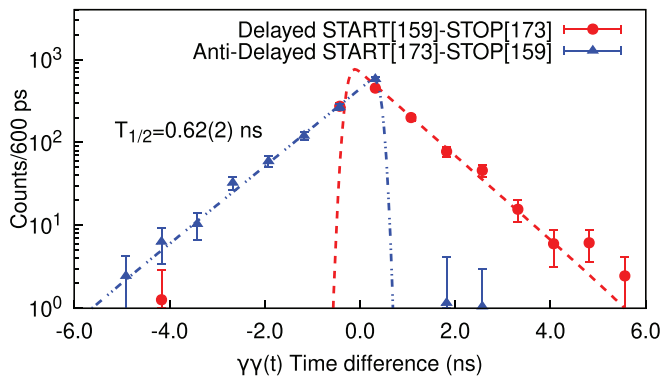
FIG. 10. Time-delayed distributions between the two LaBr$_3$(Ce) detectors for $\gamma\gamma$(t) events. The spectra were constructed by selecting the feeding 159-keV γ ray that feeds the level in one detector, and the 173-keV peak in the other one. Depending on the selected γ line in the START and STOP detectors, either the delayed or the antidelayed distributions were derived. The lifetime was obtained by a χ^2 fit of the whole time distribution to a Gaussian convoluted with an exponential function.

The state at 4513-keV is proposed to have $(19/2^-)$ spin-parity, being a member of the $(\nu f_{7/2}h_{11/2}^{-2})$ configuration [38]. The half-life has been obtained from $\gamma\gamma$(t) events measured between the two LaBr$_3$(Ce) detectors by selecting the 159- and 173-keV transitions; see Fig. 10. This procedure was employed instead of the $\beta\gamma\gamma$(t) method to avoid the contribution from the 4671-keV long-lived isomer. Two time distributions were obtained, corresponding respectively to the delayed combination, where the feeder γ ray was selected in the start detector, and to the antidelayed, where the selection of the γ rays was reversed. We adopt the final value of $T_{1/2} = 0.62(2)$ ns for this level from the weighted average of the values obtained from the fit of the two time distributions.

The analysis for the lifetime of the 4624-keV level is displayed in Fig. 11. The time-distributions employed for the
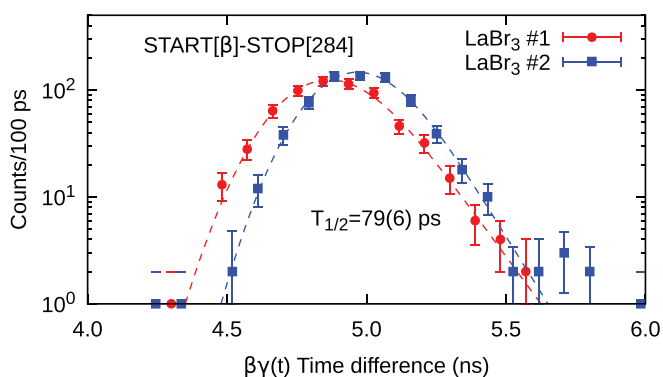
FIG. 11. Time-delayed $\beta\gamma\gamma$(t) spectra between the β and the LaBr$_3$(Ce) detectors selected by the 284-keV transition. An extra condition was required in the 2085- and 4274-keV γ lines in the HPGe detectors. The lifetime was obtained from a χ^2 fit of the whole distribution to a Gaussian-convoluted exponential function plus a constant to account for the random background using the procedure described in Ref. [59].

analysis were built using triple $\beta\gamma\gamma$(t) events, selecting the 285-keV γ ray in the LaBr$_3$(Ce) and gating on the 2085- or the 4274-keV in the HPGe detectors. The statistics of both combinations was summed in order to generate the time spectra employed in our analysis. In both scintillators, an asymmetry to the right side can be observed, which indicates a lifetime of the order of tens of picoseconds. A half-life of 79(6) ps was derived from the fit to a Gaussian-convoluted exponential function.

The lifetime analysis have been extended to the remaining observed levels that were populated with sufficient statistics. A new $T_{1/2} = 316(2)$ ns value have been obtained for the 4671-keV $(23/2^-)$ level, in agreement with previous measurements [28,37], and a new long half-live value of $T_{1/2} = 24(3)$ ns for the 4775-keV level has been measured from $\beta\gamma$(t) events between the β and the LaBr$_3$(Ce) detectors. In addition, a short lifetime of $T_{1/2} = 30(15)$ ps for the 4771-keV state, and an upper limit of $T_{1/2} = <17$ ps for the 4941-keV state. A total of seven new lifetimes measurements and one upper limit have been determined in this work.

VII. DISCUSSION

A. Position of the $\nu h_{11/2}^{-1}$ single-hole state

In this work we have performed a direct mass measurement (Sec. III) to determine the isomer energy, yielding a value of $E_x = 64.0(20)$ keV, in agreement with the previous proposal of 65.1(5) keV [27]. Additionally, we have employed a similar procedure to reference [27] to determine the $\nu h_{11/2}^{-1}$ single-hole state energy using the information from β decay. The 2369-keV γ transition is enhanced in the narrow-band $9/2^+$ laser configuration and thus its assignment to the β decay of ^{131g}In is confirmed. The 2434.1-keV level deexcites both to the ground state and to the $11/2^-$ level. This yields and excitation energy of 65.4(7) keV for the isomeric $11/2^-$ state. This is in good agreement with the value obtained from the Penning-trap mass measurement, 64(2) keV (see Sec. III). We take this value as the firm energy of the $\nu h_{11/2}^{-1}$ state in ^{131}Sn. We observe a level at 6936-keV tentatively decaying to both the $11/2^-$ state and to the 2434-keV $(7/2^+)$ level, which supports the assignment, although the confirmation via $\gamma\gamma$ coincidences is not possible due to the weak intensity of the transitions.

B. β decay of ^{131}In $\rightarrow$ ^{131}Sn

The wave functions of nuclei neighboring ^{132}Sn are dominated by single-hole configurations. The investigation of the β decay of ^{131}In (1π hole) to ^{131}Sn (1ν hole) is an excellent tool for accessing the single-particle decay strength in the region, assess the competition of GT and FF transitions and investigate the coupling to core-excited states. The different particle configurations that give rise to the three β-decaying states of ^{131}In, along with the most-likely single-particle β-decay transitions, are represented in Fig. 12.
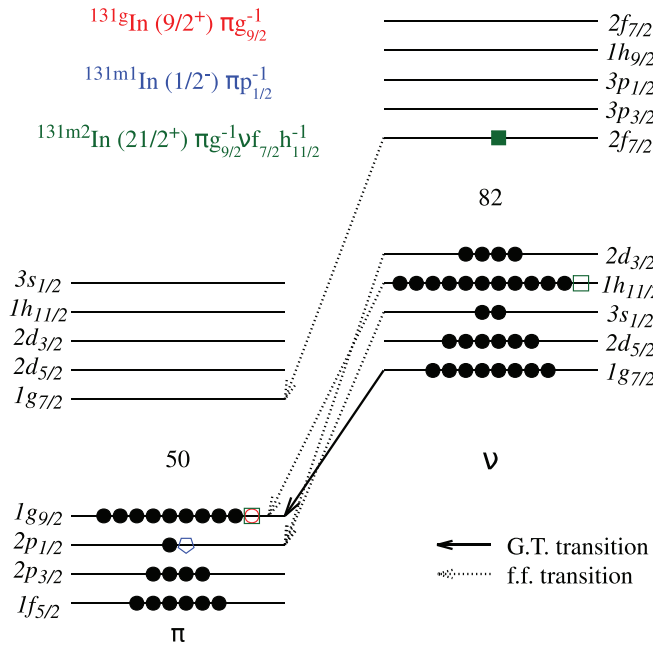
FIG. 12. Shell-model configurations of the three parent ^{131}In states and possible β-decay routes. See text for details.

1. β decay of ^{131g}In

The $(9/2^+)$ ground state of ^{131}In is associated the $\pi g_{9/2}^{-1}$ proton hole configuration. Therefore the most favorable β-decay path for this state is the allowed GT $\nu g_{7/2} \to \pi g_{9/2}$ transition. Such a GT transition is responsible for the strong feeding to the 2434-keV $(7/2^+)$ state in ^{131}Sn, which is dominated by the $\nu g_{7/2}^{-1}$ configuration. The next strongest transition would be the FF $\nu h_{11/2} \to \pi g_{9/2}$ transition, where the $11/2^-$ isomer in ^{131}Sn is directly populated. Apart from these two levels, the observation of direct population of the remaining single-particle states is expected to be minimal, owing to the higher degree of forbiddenness.

Besides these single-particle levels at low energy, the large $Q_\beta = 9240(4)$ keV makes it possible to populate high-energy states above 4 MeV, which originate from the coupling of a neutron hole with ^{132}Sn core excitations. All of the high-lying states are located at an energy about 1 to 2 MeV above the neutron separation energy and up to 7.1-MeV excitation; nevertheless, they decay via γ-ray emission. In this energy window only the 0^+ and 2^+ states in ^{130}Sn are available for decaying via neutron emission, and indeed a sizable β-delayed neutron emission probability has been observed. Above the aforementioned energy, there is a large set of medium spin states in ^{130}Sn, starting with the (7^-) isomer. These levels provide a possible path for neutron decay without a large spin difference. Considering the higher spin of the states populated in this decay $(7/2-11/2)$, the competition from the γ-ray emission branch may be helped by the large centrifugal barrier that hinders population of the 0^+ and 2^+ states via neutron emission.

2. β decay of ^{131m1}In

The $(1/2^-)$ isomer in ^{131}In is associated with the $\pi p_{1/2}^{-1}$ single-hole configuration. The β decay of this isomer leads to two FF transitions, the $\nu s_{1/2} \to \pi p_{1/2}$ and the $\nu d_{3/2} \to \pi p_{1/2}$. Therefore, the $1/2^+$ first-excited and the $3/2^+$ ground state of ^{131}Sn are expected to be predominantly populated in the decay of ^{131m1}In, as observed in our experiment.

The direct β population of the remaining single-particle levels would require forbidden transitions of second or higher order, and thus they are hindered. However, the large $Q_\beta = 9240(4)$ keV [68] opens up the possibility of feeding levels at high excitation energy, such as core-excited states, for which a low angular momentum of $J = 1/2, 3/2$ and negative parity would be expected for allowed β-decay transitions. A few of these levels are observed in the decay. We also propose a couple of tentative states with weak β feeding based on ground-state transitions; see Fig. 6.

3. β decay of ^{131m2}In

The β-decay scheme of ^{131m2}In $(21/2^+)$ shows a strong similarity to the ^{132}In decay scheme [4,27,69]. In a simple interpretation, the ^{131m2}In $(21/2^+)$ state is built by coupling the neutron hole to the ^{132}In ground state, with a $\pi g_{9/2}^{-1}\nu f_{7/2}$ configuration, leading to $\pi g_{9/2}^{-1}\nu f_{7/2}h_{11/2}^{-1}$. According to this schematic interpretation, the β decay could be factorized into two contributions: the ^{132}In decay and the $\nu h_{11/2}^{-1}$ neutron hole decay. However, once the allowed GT, and the FF transitions for the neutrons in the $h_{11/2}$ orbital are considered, only the population of very high-energy 2p3h states in ^{131}Sn would be possible, feeding core-excited configurations with two nucleons above the neutron and proton shell gaps. Thus, the decay is dominated by the GT and FF transitions from the $\pi g_{9/2}^{-1}\nu f_{7/2}$ component, analogously to the ^{132}In β decay. This similarity is reinforced by the $(21/2^+)$ spin of the isomer, which leads to the feeding of high-spin levels in ^{131}Sn that require at least one hole in the $\nu h_{11/2}$ orbital. Another factor that strengthens this resemblance is the difference in spin and parities between the parent indium state and the final tin state in both cases, ^{131m2}In $(21/2^+) \to {}^{131}$Sn $11/2^-$ ($\Delta J = 5$ and $\Delta\pi =$ yes) and ^{132}In $(7^-) \to {}^{132}$Sn 0^+ ($\Delta J = 7$ and $\Delta\pi =$ yes). In view of the analogy the particle-hole configurations of the ^{131}Sn states populated in the ^{131m2}In β decay would be the same as those in ^{132}Sn populated from ^{132}In [4] but coupled to $\nu h_{11/2}^{-1}$. Their decay paths to the $11/2^-$ state are also similar to those required in the ^{132}In decay to reach the ^{132}Sn ground state.

The negative-parity states in the range of 4–5 MeV have been interpreted as members of the $(\nu f_{7/2}h_{11/2}^{-2})$ multiplet in previous studies [27,28,38,70]. The relatively strong feeding of the $(23/2^-)$ 4671-keV member, $\log ft = 5.8$, can be understood as the FF $\nu h_{11/2} \to \pi g_{9/2}$ transition. The positive-parity states in this energy range have been identified with the $(\nu f_{7/2}d_{3/2}^{-1}h_{11/2}^{-1})$ configuration. Feeding to the levels of this multiplet should be highly suppressed due to the second degree of forbiddenness required for the $\nu d_{3/2} \to \pi g_{9/2}$ transition. The identification of new γ rays feeding these levels in this work, indicates a negligible direct β feeding compatible
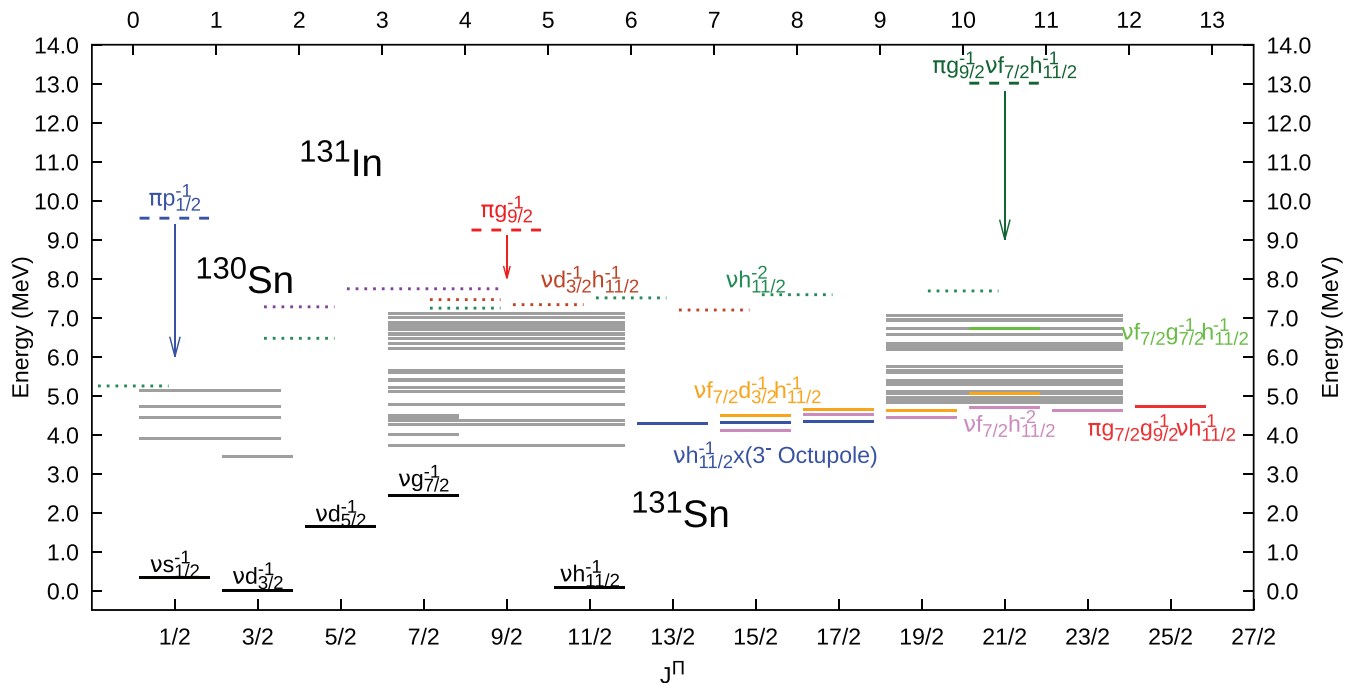
FIG. 13. Graphical summary scheme of ^{131}Sn and ^{130}Sn states populated in the β and βn decay of the three ^{131}In β-decaying states. The identified levels in ^{131}Sn and ^{130}Sn are plotted with continuous lines and dotted lines, respectively. The β-decaying states in ^{131}In are displayed with dashed lines. The color of the lines indicates the assumed configurations for the states, which is written next to them in the same color code.

with 0, solving the problem of the apparent direct β feeding reported in Refs [27,28]. The high-energy positive-parity levels at 6720 and 7054 are assigned to the $\nu f_{7/2} g_{7/2}^{-1} h_{11/2}^{-1}$ configuration in Refs. [27,28,70]. The strong β feeding to this level is interpreted as the GT $\nu g_{7/2} \rightarrow g_{9/2}$ transition. It is expected to observe a sizable population to the $(\pi g_{7/2} g_{9/2}^{-1} \nu h_{11/2}^{-1})$ configuration driven by the FF $\nu f_{7/2} \rightarrow \pi g_{7/2}$ transition. The 4775-keV state is a good candidate for this configuration, given its long lifetime of $T_{1/2} = 24(3)$ ns, which indicates a very hindered $M1$ transition to the 4671-keV level with a $(\nu f_{7/2} h_{11/2}^{-2})$ dominant configuration.

4. Feeding of states in ^{131}Sn and ^{130}Sn

In Fig. 13, the overall experimental information is presented, where the lowest-lying states of ^{130}Sn are also included. As is shown, the levels ^{131}Sn can be separated into two regions. The low-energy region below 3 MeV is characterized by a small density of levels, which can be identified with single-hole neutron states from the $N = 50$–82 shell. In the high-energy region, above 3 MeV, there is a higher density of states spanning a wide range of spins. These high-energy levels are identified as core-excited states, which are mostly based on 1p-2h configurations. In the β decay of each of the three ^{131}In isomers, a large number of states with a similar angular momenta to that of the parent isomer were populated, but several gaps can be found in the regions between the states populated by each of them. These gaps are due to the low probability of directly populating levels with $J = 5/2$, and 13/2 to 17/2. Specifically, the 2721-keV $7/2^-$ and 4045-keV $1/2^-$ states reported in Refs. [39,40] have not been observed,

neither those at 4616-keV ($5/2^-$) and 4285-keV ($13/2^+$) states.

Our data revealed the correlation between the spin of the parent ^{131}In state and the levels populated in ^{130}Sn. This can be observed in Figs. 5–7, and Table II. The β-n ^{131m1}In $1/2^-$ branch proceed mostly through the first (2^+) state, with some small feeding to states with spin up to $J = 4$. In the case of the ^{131g}In states, population of levels up to $J = 7$ is observed, being the isomeric (7^-) the one receiving most of the feeding. Most noticeable is the decay of ^{131m2}In, where only the (8^+, 10^+) are fed with sizable intensity. No population of the (2^+) nor 0^+ levels, either directly or indirectly, was observed.

5. γ decay above the S_n

One of the most interesting results is the large population of states in ^{130}Sn above the one-neutron separation energy that decay by the emission of very high-energy γ rays. Their presence was already reported earlier [28] but with no assignment to the β decay of a specific ^{131}In state. An unambiguous assignment of these new high-energy γ rays to the ^{131g}In decay is possible in our work thanks to the isomer-selective ionization. In the β decay of ^{131m1}In $1/2^-$ the population of high-energy levels up to the one-neutron separation energy was observed. In the decay of ^{131m2}In, the population of γ-emitting excited levels above S_n up to 7 MeV was observed. In this case, a number of transitions between states located above S_n can be identified. This fact suggest competition of neutron emission is rather weak for these levels. We can see a clear correlation between the upper limit for γ-emitting levels

TABLE IV. Level half-lives and reduced transition probabilities for transitions in ^{131}Sn. The $B(\lambda L)$ were calculated from the lifetimes and branching ratios obtained in this work. The theoretical conversion coefficients were taken from Bricc [62]. A pure multipolarity character for the transitions is assumed, based on the assignments from Ref. [38]. For comparison, transition rates measured for ^{132}Sn [4] are included for the analogous transitions between core-excited states.

E_i (keV)	Config$_i$	J_i^Π	$T_{1/2}$	E_f (keV)	Config$_f$	J_f^Π	E_γ (keV)	Xλ	$B(\lambda L)$ (W.u.)	Core $B(\lambda L)$ (W.u.)
331.6	$\left(\nu s_{1/2}^{-1}\right)$	$(1/2^+)$	18(4) ps	g.s.	$\left(\nu d_{3/2}^{-1}\right)$	$3/2^+$	331.6	$M1$	0.033(7)	0.036(19)[a]
4512.6	$\left(\nu f_{7/2}h_{11/2}^{-2}\right)$	$(19/2^-)$	0.62(2) ns	65.4	$\nu h_{11/2}^{-1}$	$11/2^-$	4447.2	E4	17.7(3)	7.7(4)[b]
				4168.1	$\left(\nu f_{7/2}h_{11/2}^{-2}\right)$	$(15/2^-)$	344.3	$E2$	0.59(2)	0.40(2)[c]
				4339.3	$\nu h_{11/2}^{-1} \otimes (3^-)$	$(17/2^+)$	173.3	$E1$	$6.2(6)\times 10^{-5}$	$2.57(13)\times 10^{-6}$[d]
4671.2	$\left(\nu f_{7/2}h_{11/2}^{-2}\right)$	$(23/2^-)$	316(2) ns	4512.6	$\left(\nu f_{7/2}h_{11/2}^{-2}\right)$	$(19/2^-)$	158.7	$E2$	0.340(3)	0.268(6)[e]
4771.1	$\left(\nu f_{7/2}h_{11/2}^{-2}\right)$	$(21/2^-)$	30(15) ps	4512.6	$\left(\nu f_{7/2}h_{11/2}^{-2}\right)$	$(19/2^-)$	258.2	$M1$	$2.6\left(^{+29}_{-9}\right)\times 10^{-2}$	$>6.5\times 10^{-3}$[f]
				4671.2	$\left(\nu f_{7/2}h_{11/2}^{-2}\right)$	$(23/2^-)$	99.7	$M1$	$1.8\left(^{+37}_{-11}\right)\times 10^{-1}$	$>4.6\times 10^{-3}$[g]
4774.7	$\left(\pi g_{7/2}g_{9/2}^{-1}\nu h_{11/2}^{-1}\right)$	$(25/2^-)$	24(3) ns	4671.2	$\left(\nu f_{7/2}h_{11/2}^{-2}\right)$	$(23/2^-)$	103.5	$M1$	$4.7(12)\times 10^{-4}$	$2.0\left(^{+9}_{-5}\right)\times 10^{-3}$[h]
4941.2	$\left(\nu f_{7/2}h_{11/2}^{-2}\right)$		<17 ps	4671.2	$\left(\nu f_{7/2}h_{11/2}^{-2}\right)$	$(23/2^-)$	270.2	$M1$	$>6.3\times 10^{-2}$	
4623.9	$\left(\nu f_{7/2}d_{3/2}^{-1}h_{11/2}^{-1}\right)$	$(19/2^+)$	79(6) ps	4339.3	$\nu h_{11/2}^{-1} \otimes (3^-)$	$(17/2^+)$	284.6	$M1$	$1.59(12)\times 10^{-2}$	$0.73(5)\times 10^{-2}$[i]

[a]$B(M1)$ in ^{129}Sn from Ref. [66] provided as reference.
[b]B(E4) in ^{132}Sn $(\nu f_{7/2}h_{11/2}^{-1})\, 4^+ \rightarrow\ 0^+$ g.s.
[c]$B(E2)$ in ^{132}Sn $(\nu f_{7/2}h_{11/2}^{-1})\, 4^+ \rightarrow\ 2^+$.
[d]B(E1) in ^{132}Sn $(\nu f_{7/2}h_{11/2}^{-1})\, 4^+ \rightarrow\ 3^-$ (octupole phonon).
[e]$B(E2)$ in ^{132}Sn $(\nu f_{7/2}h_{11/2}^{-1})\, 6^+ \rightarrow\ 4^+$.
[f]$B(M1)$ in ^{132}Sn $(\nu f_{7/2}h_{11/2}^{-1})\, 5^+ \rightarrow\ 4^+$.
[g]$B(M1)$ in ^{132}Sn $(\nu f_{7/2}h_{11/2}^{-1})\, 5^+ \rightarrow\ 6^+$.
[h]$B(M1)$ in ^{132}Sn $(\pi g_{7/2}g_{9/2}^{-1})\, 7^+ \rightarrow (\nu f_{7/2}h_{11/2}^{-1})\, 6^+$.
[i]$B(E2)$ in ^{132}Sn $(\nu f_{7/2}d_{3/2}^{-1})\, 5^- \rightarrow\ 3^-$ (octupole phonon).

in ^{131}Sn and the states that are available in ^{130}Sn to decay via delayed-neutron emission; see Fig. 13.

The states above S_n populated in the ^{131m1}In $1/2^-$ decay can decay to the 0^+ ground state or the 2^+ first-excited state in ^{130}Sn with a low orbital momentum $l = 0,1$. Hence, they can freely decay by neutron emission, and no γ rays emitted from excited levels above the S_n from ^{131m1}In decay were observed. On the other hand, in the decay of ^{131g}In $9/2^+$ and ^{131m2}In $(21/2^+)$, the levels have a much larger spin, $J \geqslant 7/2$, and thus the neutron needs to carry a large orbital angular momentum, $l \geqslant 3$, in order to get to the 0^+ state. Therefore, the threshold between γ-emitting, and neutron-emitting levels is shifted upwards 2 MeV above the S_n. Above this energy, states in ^{130}Sn with higher spins become available. They can be fed by neutrons emitted with low l, and this happens even from the unbound levels populated in the decay of ^{131g}In and ^{131m2}In.

6. log ft values

The apparent β feeding of to the ^{131}Sn states has been derived from the deexciting γ-ray intensities. The isomer selectivity allowed us to separate the contributions from the β decay of the ^{131g}In, ^{131m1}In, and ^{131m2}In states. As a result, a revision of the values with respect to previously reported ones is proposed, with a sizable impact on the log ft values. This solves the issue of the apparent disagreement between the different first-forbidden transition reported earlier [27,28].

Our new values indicate similar log ft values for the three FF transitions: $\nu h_{11/2} \rightarrow \pi g_{9/2}$ with log $ft = 5.49(11)$, $\nu d_{3/2} \rightarrow \pi p_{1/2}$ with log $ft = 5.37(6)$, and $\nu s_{1/2} \rightarrow \pi p_{1/2}$ with log $ft = 5.41(8)$.

C. Reduced transition probabilities in ^{131}Sn

Using the lifetimes measured in this work, along with the branching ratios, energies, and theoretical internal conversion coefficients assuming a pure multipolarity character [62], the reduced transition probabilities have been calculated. They are listed in Table IV, where the multiplet and spin-parity assignments for core-excited states from Ref. [38] have been adopted.

Regarding the enhanced $B(M1) = 0.033(7)$ W.u. rate for the $\Delta l = 2$, $\nu 3s_{1/2}^{-1} \rightarrow 3d_{3/2}^{-1}$ 331.6-keV transition, the strength is similar than that of the analogous transition in ^{129}Sn, $B(M1) = 0.036(19)$ W.u. [71]. Realistic shell-model calculations performed in Ref. [71] yielded a large enhancement of the $M1$ matrix element once the effect of core excitations was considered microscopically, pointing towards a dominant $M1$ component. Still, the enhancement for the l-forbidden $M1$ transition did not fully reproduce the much shorter than expected lifetime, most likely due to higher-order diagrams not included in the calculations.

A very similar situation in ^{131}Sn is observed here, where the single-particle nature of the involved states should be
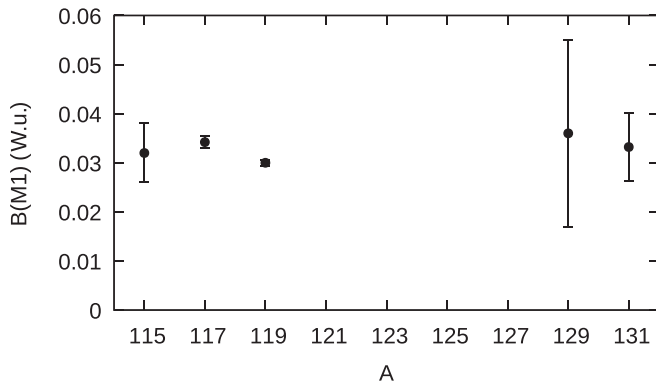
FIG. 14. Reduced transition probability $B(M1)$ for the $1/2^+ \to 3/2^+$ transitions along the tin isotopic chain. The values for $^{115-119}$Sn were taken from evaluations [74], while the value for ^{129}Sn was taken from Ref. [71].

purer. The $M1$ enhancement can only be produced by the effect of the polarization of the core. In Fig. 14, the $B(M1)$ for the $1/2^+ \to 3/2^+$ along the tin isotopic chain is shown. As is seen, the value for ^{131}Sn is in excellent agreement with that of ^{129}Sn but also with those measured in the midshell isotopes, suggesting a nearly constant behavior. Theoretical studies in the tin chain [72] pointed out the importance of proton excitations from the $\pi g_{9/2}$ orbit in order to reproduce the $B(E2)$ strength for light tin isotopes. It could be also expected that proton core excitations, such as spin-flip $g_{9/2} \to g_{7/2}$ transitions, will have a strong influence in the $M1$ transitions. The similarity between the $B(M1)$ neutron midshell and shell closure seems to support that the renormalization of the $M1$ operator for l-forbidden transitions is due to polarization of protons in the core.

It is worthwhile comparing these results to transition rates near the next double shell-closure at ^{208}Pb. The best example is the $B(M1) = 0.028(5)$ W.u. value for the $\nu 3p_{3/2}^{-1} \to \nu 2f_{5/2}^{-1}$ neutron transition in ^{207}Pb [73] but also the $B(M1) = 0.013(3)$ W.u. for the $\pi 3p_{3/2}^{-1} \to \pi 2f_{5/2}^{-1}$ proton transition in ^{207}Tl [73]. Therefore, the measured $B(M1) = 0.033(7)$ W.u. derived for the $\nu 3s_{1/2}^{-1} \to 3d_{3/2}^{-1}$ transition in ^{131}Sn, is also consistent with the systematics observed for l-forbidden $M1$ transitions in the lead region, pointing to a more general feature across the nuclear chart.

For the core-excited levels it can be observed that the $B(\lambda L)$ strengths are similar to their ^{132}Sn counterparts [4], but slightly enhanced in the case of the ^{131}Sn. The most noticeable difference is measured for the $E1$ transition from the $(\nu f_{7/2} h_{11/2}^{-2})$ to the octupole phonon state, which is more than 20 times larger than its analogous transition in ^{132}Sn. A long-lifetime, $T_{1/2} = 24(3)$ ns, has been measured for the 4775-keV state. This level deexcites via a single transition into the 4671-keV state, assigned as member of the $(\nu f_{7/2} h_{11/2}^{-2})$ multiplet. This indicates a very suppressed $M1$ between these two states, suggesting a very different structure between them, making the 4775-keV level a good candidate for the $(\pi g_{7/2} g_{9/2}^{-1} \nu h_{11/2}^{-1})$ proton particle-hole configuration.

VIII. CONCLUSIONS

The excited structure of the neutron single-hole nucleus ^{131}Sn has been investigated in detail at ISOLDE, where the ^{131}Sn excited levels were populated in the β decay of ^{131}In. Our data profited from the selective ionization by the ISOLDE RILIS to enhance the production of each particular isomer in ^{131}In and study its decay. The direct feeding of the β-decaying levels in ^{131}Sn has been derived in this work from the daughter decay intensities. The isomer selectivity allowed us to separate the contributions from the β decay of the ^{131g}In, ^{131m1}In, and ^{131m2}In states. As a result, a revision of the values with regard to previously reported ones is proposed, with a sizable effect on the $\log ft$ values. This solves the apparent disagreement between the different first-forbidden transition previously reported [27,28].

The isomer purification made it possible to obtain β-delayed one-neutron emission probabilities for the individual β-decaying states in ^{131}In, yielding $P_n[^{131g}\text{In}] = 2.4(6)\%$, $P_n[^{131m1}\text{In}] = 1.2(6)\%$, and $P_n[^{131m2}\text{In}] = 8.9(8)\%$. Moreover, the half-lives of the three β-decaying states of ^{131}In have been remeasured leading to more precise values of $T_{1/2}[^{131g}\text{In}] = 261.8(8)$ ms, $T_{1/2}[^{131m1}\text{In}] = 335.7(12)$ ms, and $T_{1/2}[^{131m2}\text{In}] = 343(4)$ ms.

An independent mass measurement has been undertaken at the IGISOL facility to determine the energy of the $1/2^-$ isomer. A definite confirmation of the excitation energy is obtained, the result being 64(2) keV. Additional evidence is found from the $\gamma\gamma$ coincidence analysis in our β-decay data, supporting the earlier tentative proposal [27] and providing a value of 65.4(7) keV for the $\nu h_{11/2}^{-1}$ single-hole state in ^{131}Sn.

The level scheme of ^{131}Sn has been expanded in this work with the addition of 31 new γ transitions and 22 new excited levels. The population of excited states in ^{131}Sn in the β-delayed neutron emission branch has also been studied.

A thorough investigation of γ-emitting excited levels placed at very high energies, above the neutron separation energies in ^{131}Sn, has been performed. There is a large number of these states in ^{131}Sn, having in some cases transitions between two neutron-unbound levels. Our analysis shows a clear correlation between the appearance of these states and the feeding β-decaying ^{131}In state. This indicates the connection between the competition of γ-ray and neutron emission with the spin of the available levels in ^{130}Sn; see Fig. 13.

The first measurements of subnanosecond lifetimes for excited states in ^{131}Sn were also performed. A short lifetime of $T_{1/2} = 18(4)$ ps the neutron single-hole 332-keV $(1/2^+)$ state has been derived, indicating an enhanced l-forbidden $M1$ character for the $\nu 3s_{1/2} \to \nu 3d_{3/2}$ transition. This finding is similar to the systematics of l-forbidden $M1$ transitions observed in the ^{208}Pb region, and the analogous transition in ^{129}Sn.

Regarding the high-spin levels, the half-lives of six new levels have been measured for the first time, and a new value has been obtained for the long-lived 4671-keV level. The transition strengths derived from these lifetimes agree very well with those of their corresponding transitions in ^{132}Sn, with the exception of the 173-keV $E1$, $4513 \to 4339$-keV transition, whose strength is ~20 times larger than the analogous $E1$

transition in ^{132}Sn. The similarity to the ^{132}In decay reinforces the interpretation of the excited states in ^{131}Sn populated in the β decay of ^{131m2}In.

[1] T. Björnstad, M. Borge, J. Blomqvist, R. Von Dincklage, G. Ewan, P. Hoff *et al.*, Nucl. Phys. A **453**, 463 (1986).

[2] K. L. Jones, A. S. Adekola, D. W. Bardayan, J. C. Blackmon, K. Y. Chae, K. A. Chipps *et al.*, Nature (London) **465**, 454 (2010).

[3] D. Rosiak, M. Seidlitz, P. Reiter, H. Naïdja, Y. Tsunoda, T. Togashi *et al.*, Phys. Rev. Lett. **121**, 252501 (2018).

[4] J. Benito, L. M. Fraile, A. Korgul, M. Piersa, E. Adamska, A. N. Andreyev *et al.* (IDS Collaboration), Phys. Rev. C **102**, 014328 (2020).

[5] P. Hoff, P. Baumann, A. Huck, A. Knipper, G. Walter, G. Marguier *et al.* (ISOLDE Collaboration), Phys. Rev. Lett. **77**, 1020 (1996).

[6] V. Vaquero, A. Jungclaus, P. Doornenbal, K. Wimmer, A. Gargano, J. A. Tostevin *et al.*, Phys. Rev. Lett. **118**, 202502 (2017).

[7] M. Piersa, A. Korgul, L. M. Fraile, J. Benito, E. Adamska, A. N. Andreyev *et al.* (IDS Collaboration), Phys. Rev. C **99**, 024304 (2019).

[8] V. Vaquero, A. Jungclaus, T. Aumann, J. Tscheuschner, E. V. Litvinova, J. A. Tostevin *et al.*, Phys. Rev. Lett. **124**, 022501 (2020).

[9] A. Kerek, G. Holm, L.-E. De Geer, and S. Borg, Phys. Lett. B **44**, 252 (1973).

[10] B. Fogelberg, M. Hellström, D. Jerrestam, H. Mach, J. Blomqvist, A. Kerek, L. O. Norlin, and J. P. Omtvedt, Phys. Rev. Lett. **73**, 2413 (1994).

[11] V. R. Pandharipande, I. Sick, and P. K. A. d. Huberts, Rev. Mod. Phys. **69**, 981 (1997).

[12] A. G. W. Cameron, J. J. Cowan, and J. W. Truran, Astrophys. Space Sci **91**, 235 (1983).

[13] A. Arcones and G. F. Bertsch, Phys. Rev. Lett. **108**, 151101 (2012).

[14] T. Kajino, W. Aoki, A. Balantekin, R. Diehl, M. Famiano, and G. Mathews, Prog. Part. Nucl. Phys. **107**, 109 (2019).

[15] J. J. Cowan, C. Sneden, J. E. Lawler, A. Aprahamian, M. Wiescher, K. Langanke, G. Martínez-Pinedo, and F.-K. Thielemann, Rev. Mod. Phys. **93**, 015002 (2021).

[16] T. Marketin, L. Huther, and G. Martínez-Pinedo, Phys. Rev. C **93**, 025805 (2016).

[17] M. Mumpower, R. Surman, G. McLaughlin, and A. Aprahamian, Prog. Part. Nucl. Phys. **86**, 86 (2016).

[18] L. Coraggio, A. Covello, A. Gargano, and N. Itaco, Phys. Rev. C **87**, 034309 (2013).

[19] A. Gargano, L. Coraggio, A. Covello, and N. Itaco, J. Phys.: Conf. Ser. **527**, 012004 (2014).

[20] P. Hoff, P. Baumann, A. Huck, A. Knipper, G. Walter, G. Marguier *et al.*, Hyperfine Interact. **129**, 141 (2000).

[21] K. L. Jones, F. M. Nunes, A. S. Adekola, D. W. Bardayan, J. C. Blackmon, K. Y. Chae *et al.*, Phys. Rev. C **84**, 034601 (2011).

[22] J. M. Allmond, A. E. Stuchbery, J. R. Beene, A. Galindo-Uribarri, J. F. Liang, E. Padilla-Rodal *et al.*, Phys. Rev. Lett. **112**, 172701 (2014).

[23] A. Korgul, P. Bączyk, W. Urban, T. Rząca-Urban, A. G. Smith, and I. Ahmad, Phys. Rev. C **91**, 027303 (2015).

[24] D. T. Yordanov, L. V. Rodríguez, D. L. Balabanski, J. Bieroń, M. L. Bissell, K. Blaum *et al.*, Commun. Phys. **3**, 107 (2020).

[25] S. Bottoni, L. Iskra, S. Leoni, B. Fornal, G. Colò, D. Bazzacco *et al.*, Acta Phys. Pol. B **50**, 285 (2019).

[26] P. Möller, B. Pfeiffer, and K.-L. Kratz, Phys. Rev. C **67**, 055802 (2003).

[27] B. Fogelberg, H. Gausemel, K. A. Mezilev, P. Hoff, H. Mach, M. Sanchez-Vega *et al.*, Phys. Rev. C **70**, 034312 (2004).

[28] R. Dunlop, C. E. Svensson, C. Andreoiu, G. C. Ball, N. Bernier, H. Bidaman *et al.*, Phys. Rev. C **99**, 045805 (2019).

[29] M. Piersa-Siłkowska, A. Korgul, J. Benito, L. M. Fraile, E. Adamska, A. N. Andreyev *et al.* (IDS Collaboration), Phys. Rev. C **104**, 044328 (2021).

[30] J. Heideman, R. Grzywacz, Z. Y. Xu, M. Madurga, J. E. Escher, T. Kawano *et al.* (IDS Collaboration), Phys. Rev. C **108**, 024311 (2023).

[31] Z. Y. Xu, M. Madurga, R. Grzywacz, T. T. King, A. Algora, A. N. Andreyev *et al.*, Phys. Rev. C **108**, 014314 (2023).

[32] Z. Y. Xu, M. Madurga, R. Grzywacz, T. T. King, A. Algora, A. N. Andreyev *et al.*, Phys. Rev. Lett. **131**, 022501 (2023).

[33] F. Kondev, M. Wang, W. Huang, S. Naimi, and G. Audi, Chin. Phys. C **45**, 030001 (2021).

[34] C. Izzo, J. Bergmann, K. A. Dietrich, E. Dunling, D. Fusco, A. Jacobs *et al.*, Phys. Rev. C **103**, 025811 (2021).

[35] V. Fedosseev, K. Chrysalidis, T. D. Goodacre, B. Marsh, S. Rothe, C. Seiffert *et al.*, J. Phys. G: Nucl. Part. Phys. **44**, 084006 (2017).

[36] L. E. De Geer and G. B. Holm, Phys. Rev. C **22**, 2163 (1980).

[37] B. Fogelberg and J. Blomqvist, Nucl. Phys. A **429**, 205 (1984).

[38] P. Bhattacharyya, P. J. Daly, C. T. Zhang, Z. W. Grabowski, S. K. Saha, R. Broda *et al.*, Phys. Rev. Lett. **87**, 062502 (2001).

[39] R. L. Kozub, G. Arbanas, A. S. Adekola, D. W. Bardayan, J. C. Blackmon, K. Y. Chae *et al.*, Phys. Rev. Lett. **109**, 172501 (2012).

[40] K. L. Jones, A. Bey, S. Burcher, J. M. Allmond, A. Galindo-Uribarri, D. C. Radford *et al.*, Phys. Rev. C **105**, 024602 (2022).

[41] I. Moore, T. Eronen, D. Gorelov, J. Hakala, A. Jokinen, A. Kankainen *et al.*, Nucl. Instrum. Methods B **317**, 208 (2013).

[42] H. Penttilä, O. Beliuskina, L. Canete, A. de Roubin, T. Eronen, M. Hukkanen *et al.*, EPJ Web Conf. **239**, 17002 (2020).

[43] P. Karvonen, I. Moore, T. Sonoda, T. Kessler, H. Penttilä, K. Peräjärvi *et al.*, Nucl. Instrum. Methods B **266**, 4794 (2008).

[44] A. Nieminen, J. Huikari, A. Jokinen, J. Äystö, P. Campbell, and E. Cochrane, Nucl. Instrum. Methods A **469**, 244 (2001).

[45] T. Eronen, V. S. Kolhinen, V.-V. Elomaa, D. Gorelov, U. Hager, J. Hakala *et al.*, Eur. Phys. J. A **48**, 46 (2012).

[46] G. Savard, S. Becker, G. Bollen, H.-J. Kluge, R. Moore, T. Otto *et al.*, Phys. Lett. A **158**, 247 (1991).

[47] S. Eliseev, K. Blaum, M. Block, C. Droese, M. Goncharov, E. Minaya Ramirez, D. A. Nesterenko, Y. N. Novikov, and L. Schweikhard, Phys. Rev. Lett. **110**, 082501 (2013).

[48] S. Eliseev, K. Blaum, M. Block, A. Dörr, C. Droese, T. Eronen *et al.*, Appl. Phys. B **114**, 107 (2014).

[49] D. A. Nesterenko, T. Eronen, A. Kankainen, L. Canete, A. Jokinen, I. D. Moore *et al.*, Eur. Phys. J. A **54**, 154 (2018).

[50] M. Wang, W. Huang, F. Kondev, G. Audi, and S. Naimi, Chin. Phys. C **45**, 030003 (2021).

[51] D. A. Nesterenko, T. Eronen, Z. Ge, A. Kankainen, and M. Vilen, Eur. Phys. J. A **57**, 302 (2021).

[52] L. M. Fraile, A. Korgul *et al.*, CERN-INTC-2015-049, INTC-P-449 (2015), https://cds.cern.ch/record/2059398.

[53] R. Catherall, W. Andreazza, M. Breitenfeldt, A. Dorsival, G. J. Focker, T. P. Gharsa *et al.*, J. Phys. G: Nucl. Part. Phys. **44**, 094002 (2017).

[54] The IDS collaboration http://isolde-ids.web.cern.ch/isolde-ids/.

[55] H. Mach, R. Gill, and M. Moszyński, Nucl. Instrum. Methods A **280**, 49 (1989).

[56] M. Moszyński and H. Mach, Nucl. Instrum. Methods A **277**, 407 (1989).

[57] L. M. Fraile, J. Phys. G: Nucl. Part. Phys. **44**, 094004 (2017).

[58] M. Piersa, A. Korgul, L. Fraile, J. Benito, E. Adamska, R. Álvarez *et al.*, Acta Phys. Pol. B **49**, 523 (2018).

[59] J. Benito, Ph.D. thesis, Universidad Complutense de Madrid, 2020.

[60] Y. Khazov, I. Mitropolsky, and A. Rodionov, Nucl. Data Sheets **107**, 2715 (2006).

[61] C. A. Stone, Ph.D. thesis, University of Maryland, 1987, https://doi.org/10.13016/dspace/f6qd-xqpa.

[62] T. Kibédi, T. Burrows, M. Trzhaskovskaya, P. Davidson, and C. Nestor, Nucl. Instrum. Methods Phys. Res., Sect. A **589**, 202 (2008).

[63] G. Lorusso, S. Nishimura, Z. Y. Xu, A. Jungclaus, Y. Shimizu, G. S. Simpson *et al.*, Phys. Rev. Lett. **114**, 192501 (2015).

[64] V. H. Phong, S. Nishimura, G. Lorusso, T. Davinson, A. Estrade, O. Hall *et al.*, Phys. Rev. Lett. **129**, 172701 (2022).

[65] A. Arima, H. Horie, and M. Sano, Prog. Theor. Phys. **17**, 567 (1957).

[66] R. Lică, H. Mach, L. M. Fraile, A. Gargano, M. J. G. Borge, N. Mărginean *et al.* (IDS Collaboration), Phys. Rev. C **93**, 044303 (2016).

[67] V. Paziy, L. M. Fraile, H. Mach, B. Olaizola, G. S. Simpson, A. Aprahamian *et al.*, Phys. Rev. C **102**, 014329 (2020).

[68] B. S. Wang, S. A. Caldwell, N. D. Scielzo, A. Czeszumska, J. A. Clark, G. Savard *et al.*, Phys. Rev. C **101**, 025806 (2020).

[69] K. Whitmore, C. Andreoiu, F. H. Garcia, K. Ortner, J. D. Holt, T. Miyagi *et al.*, Phys. Rev. C **102**, 024327 (2020).

[70] H.-K. Wang, Y. Sun, H. Jin, K. Kaneko, and S. Tazaki, Phys. Rev. C **88**, 054310 (2013).

[71] R. Lică, G. Benzoni, A. I. Morales, M. J. G. Borge, L. M. Fraile, H. Mach *et al.*, J. Phys. G: Nucl. Part. Phys. **44**, 054002 (2017).

[72] T. Togashi, Y. Tsunoda, T. Otsuka, N. Shimizu, and M. Honma, Phys. Rev. Lett. **121**, 062501 (2018).

[73] F. Kondev and S. Lalkovski, Nucl. Data Sheets **112**, 707 (2011).

[74] National nuclear data center (NNDC), http://www.nndc.bnl.gov.